# ENCLOSURE 2

# FLN-2007- 028

# NEDO-33376 LANCR02 Lattice Physics Model Description, September, 2007

## Non-Proprietary

### IMPORTANT NOTICE

This is a non-proprietary version of Enclosure 1 to FLN-2007-028, from which the proprietary information has been removed. Portions of the enclosure that have been removed are indicated by open and closed brackets as shown here [[ ]]

Global Nuclear Fuel
A Joint Venture of GE, Toshiba, & Hitachi

3901 Castle Hayne Road
Wilmington, NC 28401

**NEDO-33376**
**Revision 0**
**Class I**
**eDRF-0000-0072-2118**
**September 2007**

# Licensing Topical Report

## LANCR02 LATTICE PHYSICS MODEL DESCRIPTION

## Non-proprietary Notice

This is a non-proprietary version of NEDC-33376P, from which the proprietary information has been removed. Portions of the document that have been removed are indicated by open and closed double square brackets as shown here [[ ]].

## Legal Notice

# Table of Contents

# 1. INTRODUCTION

## *1.1. Purpose and scope*

LANCR02 is an Engineering Computer Program (ECP) that enables the detailed nuclear design and evaluation of BWR fuel lattices using a characteristics transport method as the basis for solution. LANCR02 incorporates features that support design, evaluation, and verification of the nuclear characteristics of BWR fuel lattices.

## *1.2. Features*

The function of LANCR02 is to compute the lattice nuclear characteristics and to generate the fuel assembly nuclear parameters for use in downstream applications, such as 3-D nodal simulators and transient analysis codes.

## *1.3. The LANCR02 Code System*

LANCR02 is written as a collection of individual modules. Each module performs a specific function and information is passed from one module to the next using Module program units. LANCR02 modules and their functions are as follows:

User Input Module

This module reads a set of FORTRAN Namelist input consisting of geometry inputs, enrichment location assignments, all available switches and input data, lattice state conditions, geometry descriptions, as well as rod locations.

Geometry Setting Module

This module prepares the geometrical data required for subsequent calculations in LANCR02. Variables for defining cell boundaries, geometrical configuration within cells, and material compositions are provided.

Cross Section Processing Module

This module reads the CEDAR formatted fine-group neutron cross section library for all requested isotopes.

Spectrum Calculation Module

This module calculates weighting functions (i.e., flux spectra) that will be used to condense the fine-group macroscopic cross sections to a coarser energy group structure for the two-dimensional transport calculation.

Neutron Transport Module

This module solves the two-dimensional Boltzmann transport equation using the Method of Characteristics to obtain a detailed flux distribution in each region of the lattice.

Gamma Transport Module

This module calculates a gamma source distribution using the neutron flux distribution obtained from the coarse group neutron transport module. The fixed-source Boltzmann transport equation is solved using the Method of Characteristics to obtain a detailed gamma flux in each region of the lattice. The gamma distribution is used to determine the gamma energy deposition in each region of the lattice and a gamma detector response in the SE corner of the lattice.

Output Module

This module provides all the output quantities needed by the core simulator, as well as ASCII output for printing.

Depletion Module

This module performs isotopic depletion calculations for either the fuel materials in fuel rods or the poison materials ($B^{10}$ and Hf) in control blades, or both.

# 2. METHODOLOGY

This section of the report presents a description of the theory and models that form the computational basis for LANCR02. Qualification of the methodology is part of the LANCR Lattice Physics Qualification LTR (NEDC-33377P). The application methodology is included in the LANCR/AETNA Application for Steady-state Nuclear Methods LTR (NEDC-33382P).

## *2.1. Fine-group cross-sections*

The LANCR02 calculation begins by retrieving microscopic cross section data from an accompanying fine group, energy-dependent cross section library. The entire library includes more than 100 energy groups and more than 200 individual isotopes and mixtures [1]. A list of the isotopes and the details of the LANCR02 libraries is included in the qualification LTR.

This sub-section describes the method used for obtaining microscopic cross sections from the library for each isotope in each material region of the lattice.

The multi-group cross section library for LANCR02 can be created by a standard method such as NJOY [2]. To produce a multi-group library from the continuous energy data, a flux spectrum is needed to combine pointwise data over an energy range,

$$\sigma_x^g = \frac{\int_E^{E+\Delta E} \sigma_x(E)\phi(E)dE}{\int_E^{E+\Delta E} \phi(E)dE} \tag{1}$$

where $x$ is a reaction type (e.g., fission, capture, etc.); g is a fine energy group covering the energy interval $\Delta E$; $\sigma_x(E)$ is the microscopic cross section at energy point E; and $\phi(E)$ is the flux spectrum used to weight the continuous energy cross section over the energy interval from E to $E+\Delta E$.

The flux in Eq. (1) is meant to represent the spectrum found in a typical BWR. To obtain this, it is assumed that the magnitude of the flux is inversely proportional to the energy of the neutrons,

$$\phi(E) \propto \frac{1/E}{\sigma_{t,iso}(E)+\sigma_0} \tag{2}$$

where $\sigma_{t,iso}(E)$ is the microscopic total cross section for the isotope under consideration, *iso*; and $\sigma_0$ is a microscopic background cross section. Eq. (2) is often referred to as the Bondarenko model and is based on the Narrow Resonance (NR) approximation. The total cross section in the denominator of Eq. (2) is used to create flux dips surrounding resonances, while the background cross section is used to account for scattering by all other isotopes in

the fuel mixture and may be thought of as a dilution factor of $\sigma_{t,iso}(E)$. That is, the larger the value of $\sigma_0$ becomes, the more "dilute" the value of $\sigma_{t,iso}(E)$ becomes in the sum of $\sigma_{t,iso}(E)+\sigma_0$. When $\sigma_0 \gg \sigma_{t,iso}(E)$, the value of $\sigma_{t,iso}(E)$ is insignificant and this condition is referred to as being "infinitely dilute."

For each isotope in the LANCR02 cross section library, the NR approximation is used to create a base cross section set at 293K for infinitely dilute conditions by setting $\sigma_0$ equal to a very large value in Eq. (2) (i.e., $\sigma_0 \gg \sigma_{t,iso}(E)$, representing a resonance absorber present in such small abundance that the resonances do not affect the flux spectrum). In addition, correction factors to the infinitely dilute base values are used to account for changes in the cross sections caused by different temperatures and different background cross sections (i.e., different moderating strengths). In LANCR02, these correction factors are referred to as f-tables, $f(T,\sigma_0)$ [2]. When LANCR02 obtains microscopic cross sections from the cross section library, the code reads the infinitely dilute values and enters the f-tables to obtain the appropriate correction factor as a function of temperature and microscopic background cross section,

$$\sigma^g_{x,iso} = \sigma^g_{x,iso}(293K,\infty)\cdot f^g_{x,iso}(T,\sigma_0) \tag{3}$$

Interpolation in the f-tables is performed as a quadratic function of the square root of the fuel temperature, $\sqrt{T_f}$, and the logarithm of the microscopic background cross section, $\log(\sigma_0)$. Self-shielded data for each resonance absorber are generated at different temperatures and at different background cross section conditions between 10 barns and $10^{10}$ barns (i.e., infinitely dilute).

## *2.2. Obtaining Effective Resonance Data from the Cross Section Library*

### 2.2.1. Calculation of Background Cross Sections

In order for LANCR02 to use the resonance data contained in the cross section library, the f-tables must be entered with the proper microscopic background cross section for each isotope in each fuel mixture. The task, then, is to calculate an accurate value of the microscopic background cross section.

The microscopic background cross section for any particular isotope, $\sigma_{0,iso}$, is obtained from the macroscopic background cross section for the fuel mixture as a whole, $\Sigma_0$, using the relationship,

$$\sigma_{0,iso} = \frac{\Sigma_0}{N_{iso}} - \sigma_{p,iso} \tag{4}$$

where $N_{iso}$ is the number density of isotope *iso*; and $\sigma_{p,iso}$ is the microscopic potential scattering cross section for isotope *iso*.

The calculation of a macroscopic background cross section for an isolated fuel pin is separated into two components: (1) a volume component, $\Sigma_p$; and (2) a surface component, $\Sigma_e$. The macroscopic background cross section is the sum of the two components [3], $\Sigma_0 = \Sigma_p + \Sigma_e$.

The volume component accounts for neutrons that are scattered into a resonance energy by the fuel material and is expressed as the sum of the potential scattering cross sections for all isotopes in the fuel mixture,

$$\Sigma_p = \sum_{iso} N_{iso} \sigma_{p,iso} \tag{5}$$

The potential scattering cross section is energy-independent and represents the forces that act upon a neutron as it moves in or near the nucleus. It is a function only of the effective scattering radius of the nucleus, which depends on the way in which the different wavelengths of the incident neutron (e.g., s-wave, p-wave, etc.) interact with the target nucleus. The effective scattering radius of each isotope is obtained from the ENDF/B files and the potential scattering cross section is then calculated as,

$$\sigma_{p,iso} = 4\pi R_{0,iso}^2 \tag{6}$$

where $R_{0,iso}$ is the effective scattering radius of the nuclide.

The surface component of the macroscopic background cross section accounts for neutrons that escape the fuel pellet and are scattered into a resonance energy by the surrounding moderator. The neutrons then have a finite probability of re-entering the fuel pellet and being absorbed. The surface component for an isolated fuel pellet can be approximated using the Wigner rational expression [4], where the macroscopic escape cross section, $\Sigma_e$, is expressed as the inverse of the mean chord length for a simple convex body,

$$\Sigma_e = \left(\frac{4V}{S}\right)^{-1} = \frac{1}{2r} \tag{7}$$

where V refers to the volume of the fuel pellet; S refers to the pellet surface area; and r is the pellet radius. The mean chord length for a pellet subdivided into multiple annular rings is calculated following the method outlined in [5].

The Wigner rational expression is an excellent approximation for certain applications, however it has its limitations. For typical LWR analysis, errors in the Wigner rational expression can lead one to enter the pre-processed resonance tables in the wrong location. For such applications, the Wigner approximation is typically augmented with a Bell or Levine

factor to produce more acceptable results. This is the method employed in LANCR02, where the appropriate Bell factor is determined from Monte Carlo analysis.

### 2.2.2. Dancoff Factors

The Wigner rational expression in Eq. (7) is applicable only to an isolated fuel pellet. For an array of tightly packed fuel pins, some neutrons may escape from one pellet and suffer their first collision in a neighboring pellet rather than in the surrounding moderator. This shadowing effect will alter the Wigner rational expression from that for an isolated fuel pin and is taken into account through the use of a Dancoff factor, $\Gamma$. The Dancoff factor is calculated using Sugimura and Yamamoto's neutron current method [6] and applied to the escape cross section. The new expression for the macroscopic background cross section becomes,

$$\Sigma_0 = \Sigma_p + \Gamma \Sigma_e^{isolated} \tag{8}$$

In the neutron current method, Dancoff factors are evaluated using flux values obtained from two separate solutions. The first solution is a fixed source calculation on the entire lattice in the bundle's true geometry. The second solution is a fixed source calculation on an isolated pin cell. The isolated pin cell problem supplies the reference flux for an unshielded fuel pin. The lattice calculation supplies the shielded flux for each pin location in the bundle.

The Dancoff factor can be expressed in terms of the Dancoff correction, C,

$$\Gamma = 1 - C \tag{9}$$

The Dancoff correction is defined in terms of the number of neutrons that enter the surface of the fuel pin from the moderator region. For an isolated fuel pin with a fixed source of neutrons in the moderator region, the number of neutrons entering the surface of the pin can be represented as $I_0$. For fuel pins in a bundle, the neighboring fuel pins will shield each other to some extent and the number of neutrons entering the pin surface can be represented by $I$, which will be somewhat smaller than $I_0$. The definition of the Dancoff correction is calculated as the ratio of the two surface currents,

$$C = \frac{I_0 - I}{I_0} \tag{10}$$

If we assume that the fuel pins are entirely black to all resonance neutrons (i.e., all neutrons that reach the fuel pin are absorbed), then the surface currents are independent of the moderator source intensity and we can express the Dancoff correction in terms of the flux in the fuel pins rather than the surface currents, to wit,

$$C = \frac{\phi_0 - \phi}{\phi_0} \tag{11}$$

For application in LANCR02, the fluxes in Eq. (11) are solved using the MoC transport module, which is described in Section 3 of this report. The transport solver is called twice – once to perform a fixed source calculation on the entire lattice, and once to perform a fixed source calculation on an isolated fuel pin. In both calculations, fixed sources are placed in all regions of the problem other than the fuel regions. The sources are normalized such that $S/\Sigma = \gamma$, where $S$ is the source strength in a region of the problem; $\Sigma$ is the total cross section in the region; and $\gamma$ is an arbitrary constant. For such a definition, the sources in each region of the problem will be given by $S = \gamma \cdot \Sigma$, where the constant is totally arbitrary and is uniform over the entire problem domain. After performing both fixed-source calculations, Dancoff corrections for every fuel pin location are calculated using Eq. (11) and the corresponding Dancoff factor for each pin location in the lattice is calculated using Eq. (9). If the lattice contains fuel rods of different dimensions, then the isolated pin cell calculation is performed once for each unique rod.

[[

]]

### 2.2.3. Final Background Cross Sections

For each isotope in the fuel mixture, the associated microscopic background cross section is calculated using Eqs. (4) and (8). The microscopic background cross section is then used to enter the resonance tables and obtain the appropriate cross sections for each resonance absorber isotope in each fuel mixture in the lattice.

The method described in this sub-section is a very simple technique for obtaining background cross sections. There are much more elaborate techniques used in other lattice physics codes [7]. Nevertheless, with an appropriate value of Bell factor, this simple technique used in LANCR02 is very accurate for BWR applications and produces cross sections in the resonance energy range that are in good agreement with cross sections created from MCNP reference solutions.

## *2.3. Resonance Interference Effects*

Resonance interference (RI) effects between different resonance absorbers in the same fuel mixture may be taken into account through a separate calculation in LANCR02 based on a resonance interference factor (RIF) method closely related to a method outlined in [8]. This model corrects for the fact that RI effects are not included in the fine-group cross section library.

For this calculation, a separate ultra-fine group cross section library is utilized that contains tens of thousands of groupwise data points in the resolved resonance energy range from 10 eV to 10 keV. The NR approximation is used to generate a unique flux spectrum for each resonance absorber in the fuel mixture, $\phi_{iso}^{h}$, and a separate flux spectrum for the mixture as a whole, $\phi_{Mix}^{h}$, where *h* represents an ultra-fine energy group; *iso* represents a resonance absorber isotope; and *Mix* represents the entire fuel mixture of all resonance absorber isotopes. The NR approximation assumes that the energy lost by a neutron suffering a scattering collision is large compared to the width of a resonance. Under such conditions, an insignificant number of neutrons will experience more than a single collision within any resonance and are therefore, likely to avoid resonance absorption. This approximation is very good for neutron energies above 50 eV. Below 50 eV, the approximation is less accurate, but still adequate for our needs since the most of the resonance regions for the isotopes of interest are above 50 eV.

The ultra-fine group flux for each isotope, $\phi_{iso}^{h}$, and for the fuel mixture as a whole, $\phi_{Mix}^{h}$, are described by the following expressions,

$$\phi_{iso}^{h} \propto \frac{1/E^{h}}{N_{iso}(\sigma_{t,iso}^{h}+\sigma_{0,iso})} \tag{12}$$

$$\phi_{Mix}^{h} \propto \frac{1/E^{h}}{\Sigma_{t,Mix}^{h}+\Sigma_{0}} \tag{13}$$

where $\sigma_{t,iso}^{h}$ is the ultra-fine group microscopic total cross section for isotope m; $\sigma_{0,iso}$ is the microscopic background cross section for isotope iso; $\Sigma_{t,Mix}^{h}$ is the ultra-fine group macroscopic total cross section for the fuel mixture as a whole; and $\Sigma_{0}$ is the macroscopic background cross section for the fuel mixture as a whole.

Eqs. (12) and (13) may be solved directly using the macroscopic background cross section for the fuel pellet, $\Sigma_{0}$ from Eq. (8), and the corresponding microscopic background cross sections for the individual isotopes in the fuel mixture. The fluxes from Eq. (12) are used to create parallel sets of cross sections, for each resonance absorber in the fuel mixture, in the fine-group energy structure of the LANCR02 cross section library,

$$\sigma_{x,iso}^{g} = \frac{\sum_{h\in g}\sigma_{x}^{h}\phi_{iso}^{h}}{\sum_{h\in g}\phi_{iso}^{h}} \tag{14}$$

The flux from Eq. (13) is used to create cross sections for the fuel mixture as a whole,

$$\sigma_{x,Mix}^{g} = \frac{\sum_{h \in g} \sigma_x^h \phi_{Mix}^h}{\sum_{h \in g} \phi_{Mix}^h} \tag{15}$$

where $x$ is the reaction type; iso is a resonance absorber; $g$ is the energy group structure of the LANCR02 fine-group cross section library; and $h$ is the energy group structure of the ultra-fine group cross section library. Resonance interference correction factors are then calculated, for each resonance absorber in the fuel mixture, as the ratio of Eq. (15) to Eq. (14),

$$RIF_{x,iso}^{g} = \frac{\sigma_{x,Mix}^{g}}{\sigma_{x,iso}^{g}} \tag{16}$$

The RI correction factors are applied to the cross sections from the LANCR02 fine-group library,

$$\sigma_{x,iso}^{g} = \sigma_{x,iso}^{g}(293K, \infty) \cdot f_{x,iso}^{g}(T, \sigma_0) \cdot RIF_{x,iso}^{g} \tag{17}$$

LANCR02 calculates RI correction factors for capture, fission, and elastic scattering cross sections for each major resonance absorber in the fuel (i.e., all major uranium isotopes, plutonium isotopes, and gadolinium isotopes). The implementation of the RIF method in LANCR02 is described in more detail in [9]. The effect of the RI calculation on the final result from the lattice physics code is very small and serves to basically improve fidelity in voided conditions, since the magnitude of the effect increases as the flux spectrum hardens. The RIF method increases the computation cost significantly, although the option can be engaged via input parameters.

### *2.4. Energy Condensation*

Once microscopic cross sections have been obtained from the cross section library and LANCR02 has created the macroscopic cross sections for each material region in the lattice, the code is ready to determine the flux distribution. Solution to the Boltzmann transport equation in the fine-group energy structure of the cross section library is supported in LANCR02, but the calculation is very time consuming and does not necessarily yield a significant benefit in accuracy.

A reduction in the solution can be obtained by condensation of the macroscopic cross sections from the fine-group energy structure to a more manageable smaller transport energy group structure,

$$\Sigma_{x,i}^{G} = \frac{\sum_{g \in G} \Sigma_{x,i}^{g} \tilde{\phi}_i^g}{\sum_{g \in G} \tilde{\phi}_i^g} \tag{18}$$

where $\Sigma_{x,i}^{G}$ and $\Sigma_{x,i}^{g}$ are the macroscopic cross sections of reaction $x$ for the transport group and fine-group structures, respectively. The weighting function $\tilde{\phi}_i^g$ is an approximation to the flux in region $i$ generated by a two-step process that consists of a series of one-dimensional pin cell calculations followed by a fast two-dimensional coupling calculation. Both calculations are performed in the fine-group energy structure of the LANCR02 cross section library. Although the two step-method does not necessarily produce accurate flux solution, it will give accurate relative fine group fluxes which can be used as weighting functions for the condensation. This sub-section is used to describe the methodology behind the condensation scheme.

### 2.4.1. One-Dimensional Pin Cell Spectral Calculations

Each pin cell in the lattice – including water rods and empty cells (i.e., vanish locations) - takes part in its own unique one-dimensional pin cell spectral calculation. The flux in the system is determined by solving the integral form of the transport equation using the method of collision probabilities (CP) [11], [12]. The CP method is ideal for physically small systems containing a small number of material regions and a limited number of mesh. For each pin cell calculation, the square coolant region of each cell is cylindricalized by preserving volume. A buffer zone, made up of lattice-averaged fuel and moderator material, is added to the outside of each cell to help drive the flux across inert pins and pins containing strong absorbers (e.g., gadolinium), as illustrated in Figure 2.1. The pin cell system is represented as a fixed source problem, where the fission spectrum is used as the neutron source and is placed only in the buffer zone. This helps to facilitate a speedy convergence to the transport solution without affecting the final flux spectrum.

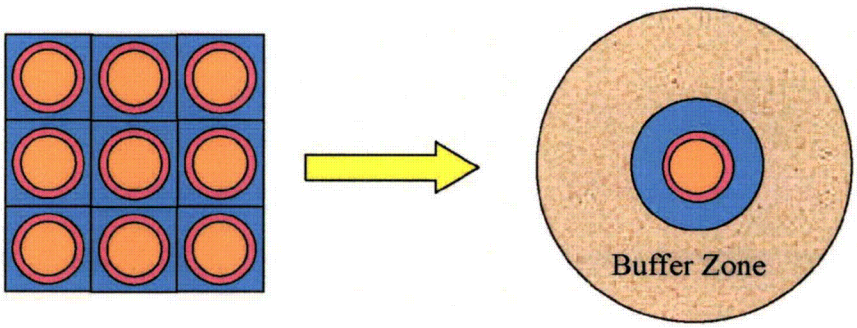


**Figure 2.1 Geometry of a pin cell with a buffer zone attached to the outside**

The scalar flux is determined by solving the following integral equation,

$$\phi(\vec{r}_i, E) = \int_V Q(\vec{r}_j, E) \cdot T(\vec{r}_j \rightarrow \vec{r}_i, E) \cdot dV_j \qquad (19)$$

where $Q(\vec{r}_j, E)$ is the neutron source in mesh $j$; and $T(\vec{r}_j \rightarrow \vec{r}_i, E)$ is the first-flight transmission probability (i.e., flux contribution) of neutrons from mesh $j$ to mesh $i$, given by the expression,

$$T(\vec{r}_j \rightarrow \vec{r}_i, E) = \frac{e^{-\tau(\vec{r}_i - \vec{r}_j, E)}}{4\pi \left| \vec{r}_i - \vec{r}_j \right|^2} \tag{20}$$

Here $\tau(\vec{r}_i - \vec{r}_j, E) = \int_0^{|\vec{r}_i - \vec{r}_j|} \Sigma_t(\vec{r}_i - \vec{\Omega}s, E) \cdot ds$ is the optical path between mesh $j$ and mesh $i$ in the neutron's direction, $\vec{\Omega}$.

In order to arrive at the expression for the scalar flux in Eq. (19), the source term is assumed to be constant across a mesh (i.e., flat flux/flat source approximation) and isotropically distributed in angle. The assumption of an isotropic source necessitates the use of transport-corrected cross sections in order to account for anisotropic scattering effects. To arrive at the transport-correction, we first expand the flux using Legendre polynomials and keep only the first two terms from the resulting expression for the spherical harmonics form of the transport equation. This leads us to the diffusion equations for the scalar flux, $\phi^g$, and current, $J_1^g$, and the corresponding definition for the diffusion coefficient,

$$D^g = \frac{1/3}{\Sigma_{t_1}^g - \sum \Sigma_{s_1}^{g' \rightarrow g} \left( J^{g'} / J^g \right)} \tag{21}$$

The denominator in Eq. (21) is the definition for the transport cross section, which is a function of the ratio of currents in various energy groups. Since we do not know the currents in our problem *a priori*, we are forced to make the assumption that the current-induced scattering of neutrons into an energy group is approximately equal to the current-induced scattering of neutrons out of the energy group,

$$\sum_{g'} \Sigma_{s_1}^{g' \rightarrow g} J^{g'} \approx \sum_{g'} \Sigma_{s_1}^{g \rightarrow g'} J^g \tag{22}$$

This is a fair assumption when scattering is the dominant process and relatively little neutron absorption is taking place. It is a poor assumption when absorption is the dominant process, such as in a control blade or a fuel pin containing gadolinium.

From Eq. (22) it follows that,

$$\Sigma_{tr}^g = \Sigma_t^g - \sum_{g'} \Sigma_{s_1}^{g \rightarrow g'} = \Sigma_t^g - \Sigma_{s_1}^g \tag{23}$$

which is the LANCR02 definition for the transport cross section and, hence, the transport-correction. In Eq. (23), $\Sigma_t^g$ is the total cross section in group g; and $\Sigma_{s_1}^g$ is the first moment of

the total scattering cross section in group g (i.e., $\Sigma_{s_1}^g = \bar{\mu}^g \Sigma_{s_0}^g$). The transport cross section is internally created by LANCR02 from data held in the cross section

In one-dimensional cylindrical geometry, we can eliminate neutron motion in the polar direction by using our previous assumption of an isotropic source and integrating $\phi$ over z. After doing so, we are left with expressions for the transmission kernel terms that rely only on the optical distances in the plane of the problem,

$$T_{i\leftarrow j}^g = \frac{P_{i\leftarrow j}^g}{\Sigma_i^g V_i}$$

$$\Sigma_i^g V_i P_{i\leftarrow j}^g = \frac{1}{2\pi}\int d\varphi \int dy [Ki_3(\tau_{ij}^g) - Ki_3(\tau_{ij}^g + \tau_j^g) - Ki_3(\tau_{ij}^g + \tau_i^g) + Ki_3(\tau_{ij}^g + \tau_j^g + \tau_i^g)] \qquad (24)$$

where $Ki_3(\tau)$ are Bickley-Nayler functions that account for the motion of neutrons out of the plane of the problem. All CP's originating from each mesh are normalized to enforce neutron conservation. That is, a neutron born within a mesh must have a total probability equal to 1.0 of having a collision somewhere.

Specular reflection boundary conditions are used on the outside of the one-dimensional pin cell geometry to simulate perfect reflection in the square moderator system (i.e., Weigner-Seitz cell). This is accomplished using Carlvik's modification to the black boundary collision probabilities,

$$\Sigma_{tr,i}^g V_i \hat{P}_{i\leftarrow j}^g = \Sigma_{tr,i}^g V_i P_{i\leftarrow j}^g + \frac{R_j R_i}{\sum_j R_j} \qquad (25)$$

where $R_i^g = \Sigma_{tr,i}^g V_i - \sum_j \Sigma_{tr,j}^g V_j P_{i\leftarrow j}^g$ [12]. The white boundary collision probabilities, $\hat{P}_{i\leftarrow j}^g$, are used in Eq. (24) in place of the black boundary collision probabilities, $P_{i\leftarrow j}^g$.

The integrations in Eq. (24) are performed numerically using sets of parallel, equidistant tracks (spaced a distance *dy* apart), which are traced over the geometry of the system at several equally spaced azimuthal angles (distributed every $d\varphi$ radians). The collision probabilities between the various mesh and boundaries are then calculated along these tracks. In one-dimensional cylindrical geometry, the integration over angle is contained within the spatial integration, as illustrated in Figure 2.2, and only a single set of tracks need be traced over the system.

Expressing the multi-group equations of the CP method as a coupled system of linear equations, we have,

$$\phi_i^g = \sum_j T_{i\leftarrow j}^g S_j^g + \sum_j T_{i\leftarrow j}^g V_j \Sigma_{s_j}^{g\leftarrow g} \phi_j^g$$

$$S_j^g = \sum_{g'\neq g} V_j \Sigma_{s_j}^{g\leftarrow g'} \phi_j^{g'} + F_j^g$$

$$\sum_j \phi_j^g (\delta_{i,j} - \Sigma_{s_j}^{g\leftarrow g} T_{i\leftarrow j}^g V_j) = \sum_j T_{i\leftarrow j}^g S_j^g \qquad (26)$$

where $F_j^g$ is the fixed source in region j. The system in Eq. (26) can be expressed in matrix form as,

$$\underline{\underline{A}}\,\underline{\phi} = \underline{B} \qquad (27)$$

where the matrix elements are defined as,

$$a_{ij}^g = \delta_{ij} - \Sigma_{s_j}^{g\leftarrow g} T_{i\leftarrow j}^g V_j$$

$$b_i^g = \sum_j T_{i\leftarrow j}^g S_j^g$$

Solution to Eq. (27) is obtained from $\underline{\phi} = \underline{\underline{A}}^{-1}\underline{B}$, where $\underline{\underline{A}}^{-1}$ is the inversion of $\underline{\underline{A}}$, performed by Gauss-Jordan elimination before beginning the flux iterates.

The solution to Eq. (27) yields a flux spectrum in each region of each pin cell in the fine-group energy structure of the cross section library. Even though each pin cell geometry contains an outer buffer zone, the flux has been generated without considering the effects of the true surroundings on the spectrum (e.g., the effects of water gaps, water rods, strong absorber pins, control blades, etc.).

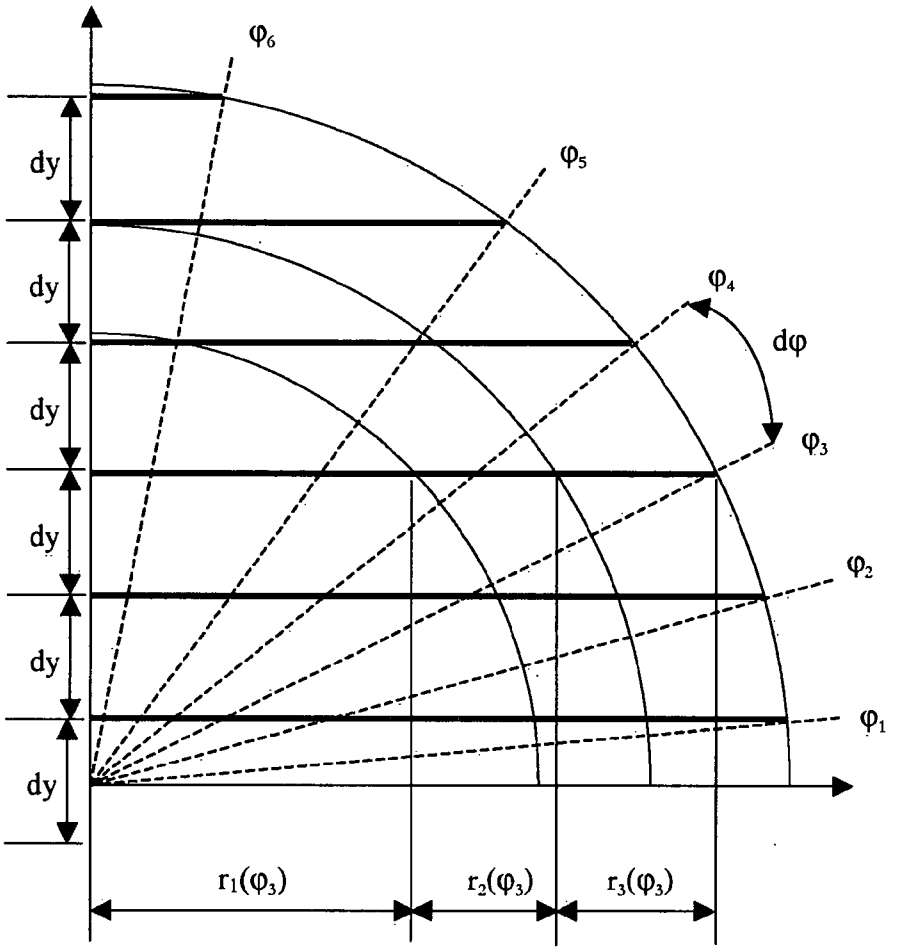


**Figure 2.2 Integration variables associated with cylindrical geometry.**

### 2.4.2. Two-Dimensional Coupling Calculation

Before condensing cross sections to smaller transport energy group structure, the spectrums from the one-dimensional pin cell calculations need to be updated to account for the effects of the true surroundings. In LANCR02, this is accomplished by performing a two-dimensional calculation on the entire lattice using a simplified geometry and a simplified solution to the transport equation.

The LANCR02 two-dimensional coupling calculation solves the integral transport equation using a response matrix (RM) method based on simplified transmission kernels [13]. Each pin cell is homogenized into an equivalent material set of cross sections using the fluxes from the 1-D pin cell calculations. Cells are coupled to each other via surface currents, which are assumed to be isotropically distributed. For an accurate solution to the transport equation, such assumptions would not be possible. However, for our purpose of generating a condensation spectrum, such assumptions are acceptable.

The equations representing the scalar flux and outward-directed currents are, respectively,

$$\phi_I^g = T_{I\leftarrow I}^g Q_I^g V_I + \sum_s T_{I\leftarrow s}^g J_{s,in}^g A_s \tag{28}$$

$$J_{s,out}^g = T_{s\leftarrow I}^g Q_I^g V_I + \sum_{s'} T_{s\leftarrow s'}^g J_{s',in}^g A_{s'} \tag{29}$$

where I represents a spatial mesh, such as a homogenized pin cell; s represents a surface to mesh $I$; the $T$'s are transmission kernels between volumes and/or surfaces; $V$ represents the volume of mesh $I$; and $A_s$ represents the surface area of surface s. Outward-directed currents from one mesh become the inward-directed currents to the neighboring mesh.

Transmission kernels are calculated by tracing streaming rays at different angles, dφ, over each individual mesh in the problem, along which the integrations to the TP expressions are performed, as illustrated in Figure 2.3. The volume-to-volume, surface-to-volume, and surface-to-surface transmission kernels are calculated as,

$$T_{i\leftarrow i}^g = \frac{1}{\Sigma_{tr_i}^g V_i} \int \frac{d\varphi}{2\pi} \int dy \cdot P_{i\leftarrow i}^g$$

$$T_{i\leftarrow s}^g = \frac{1}{\Sigma_{tr_i}^g V_i} \int \frac{d\varphi}{2\pi} \int dy \cdot P_{i\leftarrow s}^g$$

$$T_{s\leftarrow s'}^g = \frac{2}{A_{s'}} \int \frac{d\varphi}{2\pi} \int dy \cdot P_{s\leftarrow s'}^g \tag{30}$$

where the collision probabilities are expressed in terms of Bickley-Nayler functions, $Ki_3(\tau)$, just as in the CP method,

$$P_{i\leftarrow i}^g = 1 - \frac{1}{\Sigma_{tr_i}^g V_i} \left[ \frac{\pi}{4} - Ki_3(\tau_{i\leftarrow i}^g) \right]$$

$$P_{i\leftarrow s}^g = \frac{1}{2A_s} \left[ \frac{\pi}{4} - Ki_3(\tau_{i\leftarrow s}^g) \right]$$

$$P_{s\leftarrow s'}^g = \frac{1}{2A_{s'}} Ki_3(\tau_{s\leftarrow s'}^g) \tag{31}$$

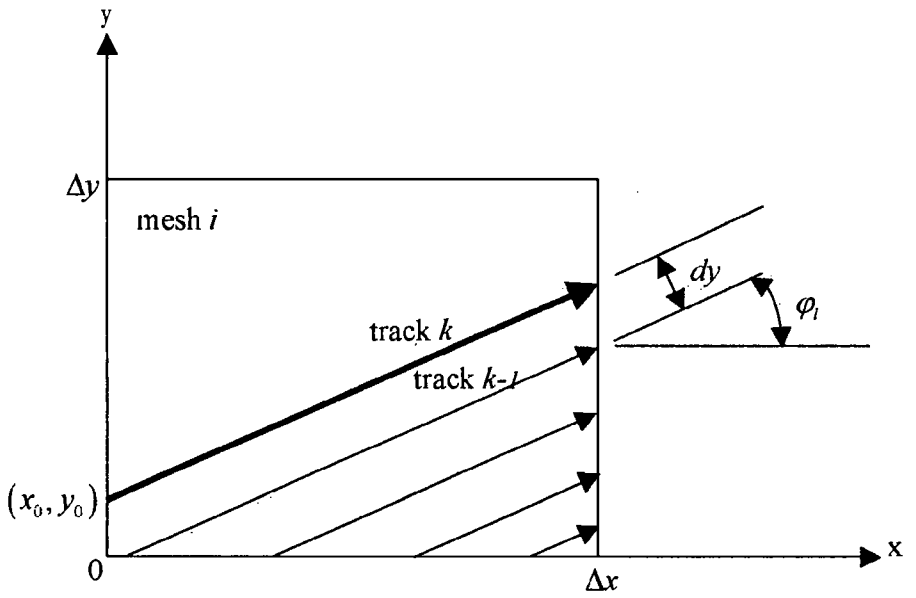


**Figure 2.3 Streaming rays traced across a mesh at a specific angle**

The CP's that originate from each mesh are normalized to enforce neutron conservation, just as is done for the pin cell calculations.

In Eq. (31), the τ's are optical distances between volumes and/or surfaces in the xy-plane of the problem. Fluxes and currents are solved using a red-black iteration scheme.

Following the completion of the coupling calculation, the energy distribution of neutrons from the 1-D pin cell calculations are updated to account for the effects of the surroundings,

$$\tilde{\phi}_i^g = \phi_i^g \cdot \frac{\phi_I^g V_I}{\sum_{i \in I} \phi_i^g V_i} \tag{32}$$

where $i$ is each region within pin cell $I$.

Fluxes for the surrounding regions of the lattice – channel box wall and water gaps – are obtained directly from the RM solution. Fluxes for the various regions of a control blade are obtained from a series of one-dimensional pin cell calculations performed on each absorber tube in a control blade and updated with the flux from the RM solution. Eq. (32) represents the flux for each material region of the problem that will be used to condense the macroscopic cross sections. The final energy group structure for the two-dimensional transport calculation depends on the accuracy of the condensation scheme, the energy group boundaries in the original fine-group energy structure of the cross section library, and the types of problems to be analyzed by the lattice physics code.

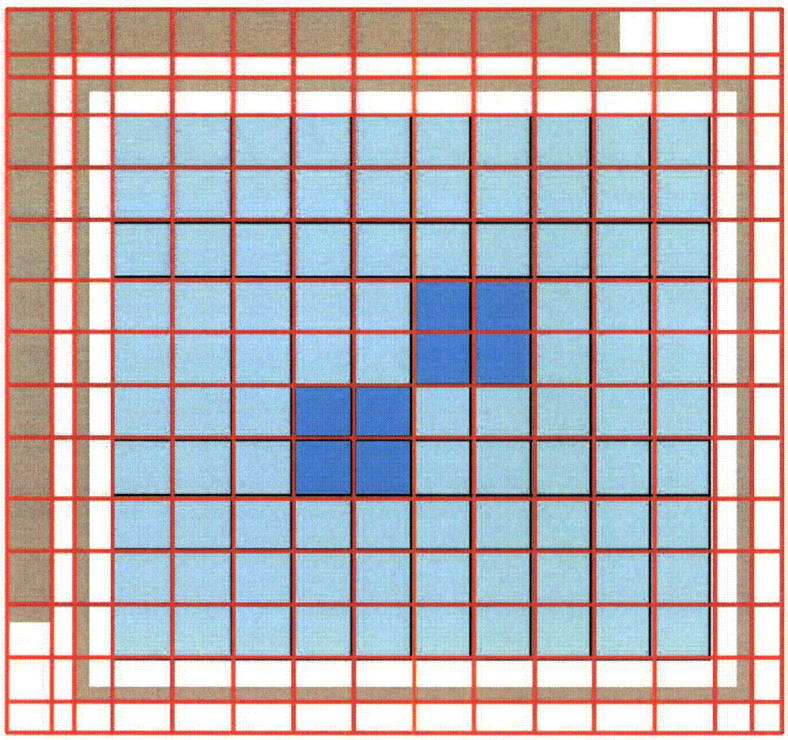

**Figure 2.4 Typical geometry of coupling calculation for a 10x10 lattice with control blade**

### *2.5. Two-Dimensional Transport Calculation*

After performing the RM calculation and collapsing the cross sections to the transport group structure, the final two-dimensional lattice calculation is performed by solving the Boltzmann transport equation, using the Method of Characteristics (MoC) [10], [14]. The multi-group, discrete angle Boltzman equation of the form,

$$\Omega_m \nabla \Phi_i^g(\Omega_m) + \Sigma_{tr,i}^g \Phi_i^g(\Omega_m) = \frac{1}{4\pi}\left[\sum_{g'} \Sigma_{s,i}^{g' \to g} \phi_i^{g'} + \frac{\chi^g}{k} \sum_{g'} \nu \Sigma_{f,i}^{g'} \phi_i^{g'}\right] \tag{33}$$

then can be expressed as,

$$\frac{d\Phi_{m,i}^G}{ds_m} + \Sigma_{tr,i}^G \Phi_{m,i}^G = Q_{m,i}^G \tag{34}$$

where $s_m$ is the length along a streaming track across a mesh at angle $\Omega_m$, $\Phi_{m,i}^G$ is the angular flux in direction $\Omega_m$, across mesh $i$, in energy group $G$; and $Q_{m,i}^G$ is the corresponding angular source, which can be calculated using transport-corrected cross sections or can model anisotropic scattering effects explicitly.

To solve the Characteristics equation (34), streaming tracks are traced over the problem geometry at a number of different angles. Each angle has associated with it a weight, and each track has associated with it a width. Solution to the Characteristics equation, in terms of the angular flux, is obtained along streaming rays and is of the form,

$$\Phi_{m,i}^{G}(s_m) = \Phi_{m,i}^{G}(0)e^{-\Sigma_{tr,i}^{G} s_m} + \frac{Q_{m,i}^{G}}{\Sigma_{tr,i}^{G}}(1 - e^{-\Sigma_{tr,i}^{G} s_m}) \tag{35}$$

where the source across a mesh is considered constant (i.e., flat source/flat flux approximation).

The scalar flux for a given mesh is calculated by integrating the angular flux along all streaming tracks that cross the mesh, and integrating over all directions of motion,

$$\phi_i^G = \int_{4\pi} \bar{\Phi}_i^G(\Omega) d\Omega = 4\pi \sum_m \bar{\Phi}_{m,i}^G \omega_m \tag{36}$$

where $\omega_m$ is the weight associated with each direction of motion; and $\bar{\Phi}_{m,i}^G$ is the average angular flux in a specific direction across a given mesh, calculated as,

$$\bar{\Phi}_{m,i}^G = \frac{\sum_k \bar{\Phi}_{m,k,i}^G \cdot s_{m,k,i} \cdot d_m}{\sum_k s_{m,k,i} \cdot d_m} \tag{37}$$

where $d_m$ is the separation between parallel streaming tracks; $s_{m,k,i}$ is the length of the streaming track crossing mesh $i$; and $k$ represents the different streaming tracks that cross mesh $i$ in direction $\Omega_m$. To obtain an expression for the average value of the angular flux along a streaming track, $\bar{\Phi}_{m,k,i}^G$, Eq.(35) is integrated along the track of motion and divided by the length of the track,

$$\bar{\Phi}_{m,k,i}^G = \frac{\int_0^{s_{m,k,i}} \Phi_{m,k,i}^G(s') ds'}{\int_0^{s_{m,k,i}} ds'} \tag{38}$$

Solution to the characteristics equation reduces to finding the intersections between rays and mesh boundaries and calculating the angular flux between intersections. The final solution to the equation produces a very detailed flux distribution throughout the lattice in the condensed transport energy group structure.

Section 3 of this report presents a much more detailed description of the MoC technique as implemented in LANCR02.

### *2.6. Fundamental Mode Calculation*

The MoC lattice calculation assumes perfect reflection on all surfaces of the bundle. In this way, there are no neutrons leaking into or out of the system. However, the data that is generated by the lattice physics code will be used in a nodal code to model an entire reactor and, within the reactor, there are almost always neutrons leaking into or out of each node in the system. To be consistent with the way in which the nodal cross sections are to be used, LANCR02 must somehow account for neutron leakage at the lattice physics level.

Leakage effects are included in an *ad hoc* way by performing a buckling calculation on the lattice. LANCR02 solves the fundamental mode equation in the diffusion approximation for an energy-independent material buckling,

$$\bar{\Sigma}_r^g \Psi^g + B_m^2 \bar{D}^g \Psi^g = \sum_{g' \neq g} \bar{\Sigma}_s^{g \leftarrow g'} \Psi^{g'} + \bar{\chi}^g \tag{39}$$

where $\bar{D}^g = 1/\left(3\bar{\Sigma}_{tr}^g\right)$ is the lattice-averaged diffusion coefficient; and $\bar{\Sigma}_r^g = \bar{\Sigma}_{tr}^g - \bar{\Sigma}_s^{g \leftarrow g}$ is the lattice-averaged removal cross section. and $\Psi^g$ is the leakage adjusted fundamental mode flux.

Eq. (39) assumes that the flux has been normalized to a single neutron being lost from the system, $\sum_g (\bar{\Sigma}_a^g + \bar{D}^g B_m^2)\Psi^g = 1$. The eigenvalue in the system is then calculated from,

$$k_{eff} = \sum_g \nu \bar{\Sigma}_f^g \Psi^g \tag{40}$$

The lattice-averaged cross sections are calculated by volume- and flux-weighting the individual cross sections from the various regions of the problem,

$$\bar{\Sigma}_x^g = \frac{\sum_i \Sigma_{x,i}^g \phi_i'^g V_i}{\sum_i \phi_i'^g V_i} \tag{41}$$

In Eq. (41), x is a reaction type and $\phi_i'^g$ is the MoC flux distribution after being expanded back to the fine-group energy structure of the cross section library,

$$\phi_i'^g = \tilde{\phi}_i^g \cdot \frac{\phi_i^G}{\sum_{g \in G} \tilde{\phi}_i^g} \tag{42}$$

The flux expansion is performed in order to more accurately capture leakage effects in the fast energy range, where most neutron leakage is occurring. In Eq. (42), $\tilde{\phi}_i^g$ is the fine-group condensation flux from Eq. (32); and $\phi_i^G$ is the transport-group flux from the MoC calculation, given by Eq. (36).

The material buckling is adjusted until $k_{eff} = 1.0$. That is, an initial calculation is performed by setting $B_m^2 = 0$. This reproduces the infinite lattice eigenvalue. Next, a second calculation is performed by setting the buckling to a very small positive value, e.g., $B_m^2 = 10^{-6}$. The eigenvalues from the first two calculations are used to extrapolate the buckling value to a new value and the corresponding eigenvalue is calculated using Eq. (40). This process continues until an eigenvalue sufficiently close to unity is obtained (i.e., $|k_{eff} - 1| < \varepsilon$). This produces the flux spectrum for a critical system and the expanded flux distribution from the MoC solution is adjusted to account for leakage effects,

$$\phi_i''^g = \phi_i'^g \cdot \frac{\Psi^g \cdot \sum_i V_i}{\sum_i \phi_i'^g V_i} \tag{43}$$

Eq. (43) represents the final flux distribution for the lattice. The leakage flux is used to create the nodal data and to deplete the burnable isotopes in the fuel.

The adjoint flux is also needed to accurately generate nodal kinetics data for the effective delayed neutron fraction, $\beta_{eff}^j$, and the prompt neutron lifetime, $l_p$,

$$\begin{aligned}\beta_{eff}^j &= \frac{\sum_{iso}\left[\sum_g \beta_{iso}^j \chi_\gamma^g \Psi^{\dagger g} \cdot \sum_g \nu\sigma_{f,iso}^g N_{iso} \Psi^g\right]}{\sum_{iso}\left\{\left(1-\beta_{iso}^j\right)\sum_g \chi_p^g \Psi^{\dagger g} + \beta_{iso}^j \sum_g \chi_\gamma^g \Psi^{\dagger g}\right\} \cdot \sum_g \nu\bar{\Sigma}_f^g \Psi^g} \\ &= \frac{\sum_{iso}\left[\sum_g \beta_{iso}^j \chi_\gamma^g \Psi^{\dagger g} \cdot \sum_g \nu\sigma_{f,iso}^g N_{iso} \Psi^g\right]}{\sum_g \bar{\chi}^g \Psi^{\dagger g} \cdot \sum_g \nu\bar{\Sigma}_f^g \Psi^g}\end{aligned} \tag{44}$$

$$l_p = \frac{\sum_g \frac{1}{v^g} \Psi^{\dagger g} \Psi^g}{\sum_g \bar{\chi}^g \Psi^{\dagger g} \cdot \sum_g \nu\bar{\Sigma}_f^g \Psi^g} \tag{45}$$

where the outer summation in Eq. (44) is over major actinides in the fuel and $j$ represents a delayed neutron group. The adjoint flux for our system is approximated by solving the adjoint to the fundamental mode equation,

$$\bar{\Sigma}_r^g \Psi^{\dagger g} = \sum_{g' \neq g} \bar{\Sigma}_s^{g \to g'} \Psi^{\dagger g'} + \nu\bar{\Sigma}_f^g \tag{46}$$

where the removal cross section now contains the leakage term, $\bar{\Sigma}_r^g = \bar{\Sigma}_{tr}^g - \bar{\Sigma}_s^{g\leftarrow g} + B_m^2 \bar{D}^g$. In this derivation, the spatial component of the adjoint flux is assumed to be equivalent to the spatial component of the forward flux and only the energy distribution of the adjoint flux is assumed to differ from that of the forward flux.

### *2.7. Gamma Transport Calculation*

LANCR02 contains an explicit gamma transport calculation that provides a detailed rod-by-rod gamma energy deposition edit, along with a gamma detector response for a detector present in the SE corner of the lattice. The gamma calculation is performed using the same MoC module as is used to solve the neutron eigenvalue problem. Steady state gamma sources are calculated for each region of the lattice in a gamma energy group structure. The gamma calculation is a fixed source calculation that uses cross sections from a gamma library, where the gamma sources, due to neutron capture and fission, are given by the following expressions,

$$q_{capture}^{\gamma} = \sum_{G} N_{iso} \sigma_{capture,iso}^{G} V_i \phi_i^G q_{capture,iso}^{\prime G} \chi_{capture,iso}^{G\rightarrow\gamma} \tag{47}$$

$$q_{fission}^{\gamma} = \chi_{fission,iso}^{\gamma} \cdot q_{fission,iso}^{\prime} \sum_{G} N_{iso} \sigma_{fission,iso}^{G} V_i \phi_i^G \tag{48}$$

Here, $q_{capture,iso}^{\prime G}$ is the gamma energy (in MeV/fission) released by neutron capture in isotope iso, neutron energy group $G$; $q_{fission,iso}^{\prime}$ is the total gamma energy (in MeV/fission) released through neutron fission in isotope iso; $\chi_{capture,iso}^{G\rightarrow\gamma}$ is the gamma spectrum that distributes the energy released from neutron capture in neutron energy group $G$, isotope *iso*, to gamma energy group $\gamma$, and $\chi_{fission,iso}^{\gamma}$ is the gamma spectrum that distributes the energy released from fission in isotope *iso*. The total fixed source in each region of the problem is the sum of Eq. (47) and Eq. (48).

The LANCR02 gamma module uses the same geometry and angular detail to solve the MoC equation as is used to determine the neutron flux distribution. The total fixed source per mesh for the MoC equation is given by,

$$q_n^{\gamma} = q_{capture,n}^{\gamma} + q_{fission,n}^{\gamma} + \sum_{\gamma'} \Sigma_{s,n}^{\gamma'\rightarrow\gamma} \phi_n^{\gamma'} \tag{49}$$

#### 2.7.1. Calculation of local gamma energy deposition

Gamma energy deposition in each unique material region of the lattice is calculated by using the converged gamma fluxes and macroscopic energy deposition cross sections,

$$E_{\gamma,i} = \sum_{\gamma} \Sigma_{e,i}^{\gamma} V_i \phi_i^{\gamma} \tag{50}$$

Eq. (50) is solved for each fuel rod individually and for other material regions as a whole. Edits are supplied for the rod-by-rod gamma energy distribution and for the energy deposited in the coolant, cladding, channel box wall, bypass region, water rods, and control blade. These edits do not include other forms of energy deposition, such as conduction through the channel wall or kinetic heating from neutron slowing down in the coolant.

### 2.7.2. Calculation of Gamma Detector Response

The detector response is currently defined as the energy deposited to the detector in Watts at the assembly average power density level defined via input. The energy deposition cross section for the detector is obtained from iron (Fe). The equation for calculating the gamma j-factor is described in Section 9 of this report.

# 3. DETAILS OF THE CHARACTERISTICS MODULE

Subsection 2.5 presented a very brief overview of the basic equations solved when implementing the MoC technique. This section will be used to describe the MoC implementation in LANCR02 in more detail. The characteristics solution has become a popular choice for lattice physics applications, and this section is used to give the reader a deeper understanding of the method that forms the foundation of the LANCR02 lattice physics code.

## *3.1. Quadrature Set*

In order to model neutron motion in the MoC technique, streaming rays (i.e., characteristics) are traced across the two-dimensional system in a number of different directions, where the accuracy of the solution depends on the total number of directions modeled and the spacing between parallel rays. The discrete directions of motion are defined using a quadrature set [15], which consists of a set of azimuthal angles and a separate set of polar angles, as illustrated in Figure 3.1. Directions of motion pass through the centroid of the solid angle subtended by the boundaries on a unit sphere. The weight associated with each direction of motion is equal to the area of the solid angle.

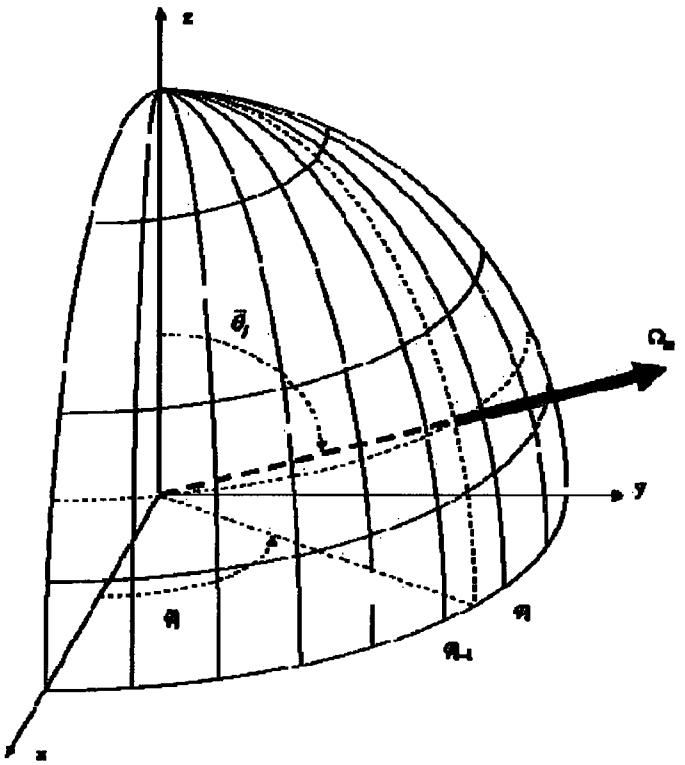

**Figure 3.1 Example of a quadrature for the MoC.**

### 3.1.1. Azimuthal Angles of Motion

The azimuthal angles of motion for LWR applications are evenly spaced in the xy-plane of the problem. For a specified number of azimuthal directions, $N_a$, the boundaries of motion are spaced at intervals $\Delta\varphi = 2\pi/N_a$ apart and the azimuthal direction of motion takes place through the center of two neighboring boundaries,

$$\bar{\varphi}_i = \frac{1}{2}(\varphi_{i-1} + \varphi_i) \tag{51}$$

where $\varphi_0 = 0$. The weight associated with each azimuthal direction of motion is equal to the area between the boundaries, $\omega_i = 2\pi/N_a$. The total weight of all azimuthal directions sums to $2\pi$.

[[

]]

### 3.1.2. Polar Angles of Motion

The polar directions of motion are distributed using the Tabuchi-Yamamoto optimal quadrature set [15]. The code also contains several Legendre quadrature sets that can be chosen by the user via input parameters. There are 3 separate optimal quadrature sets and six separate Legendre quadrature sets to choose from in the LANCR02 MoC module. The optimal quadrature sets have been obtained from [15], while the Legendre quadrature sets have been obtained directly from [13].

[[

]]

### 3.1.3. Adjusting Angles and Separation Distances to Align Tracks Along Boundaries

In two-dimensional problems, tracks reflect off the north and south boundaries of the problem, as well as off the east and west boundaries to the problem. This leads to unique azimuthal angles of motion between $0 \le \bar{\varphi} \le \pi/2$, and three reflected angles of motion

between $\pi/2 \le \bar{\varphi} \le 2\pi$ – one reflected angle in each directional quadrant of the problem. In order to produce an exact solution to the characteristics equation, the end of each incident angle must align precisely with the beginning of its reflected counterpart along the problem boundary.

To ensure perfect reflection in two dimensions, track separations and streaming angles in the xy-plane of the problem are altered slightly based on the overall dimensions of the problem. If the system is of total width $X$ and total height $Y$, then the total number of system widths spanned by a characteristic moving in the azimuthal direction of motion $\bar{\varphi}_i$, with a characteristic separation, $d_i$, is,

$$nx_i = \left| \frac{X \cos \bar{\varphi}_i}{d_i} \right| \tag{52}$$

and the total number of system heights spanned is,

$$ny_i = \left| \frac{Y \sin \bar{\varphi}_i}{d_i} \right| \tag{53}$$

In order to ensure that all tracks in direction $\bar{\varphi}_i$ align with their reflective counterparts along the boundary of the system, $nx$ and $ny$ are rounded up to the nearest integer values and the updated angle of streaming is re-calculated as,

$$\bar{\varphi}_i' = \tan^{-1}\left( \frac{ny_i' \cdot Y}{nx_i' \cdot X} \right), \text{ where } nx_i' = \text{int}(nx_i + 1) \text{ and } ny_i' = \text{int}(ny_i + 1) \tag{54}$$

along with the updated separation distance,

$$d_i' = \frac{X \cdot Y}{\sqrt{(ny_i' \cdot Y)^2 + (nx_i' \cdot X)^2}} \tag{55}$$

Using these angles and separations, the azimuthal set of parallel, equidistant tracks are traced across the system at angles between $0 \le \bar{\varphi}_i' \le \pi$. For angles of motion between $\pi \le \bar{\varphi}_i' \le 2\pi$, the previous tracks are used, allowing neutrons to travel in the opposite direction.

### *3.2. Ray Tracing*

Cyclic trajectory ray tracing in LANCR02 is based on a method described in [10]. The ray tracing routine in LANCR02 begins by laying a Cartesian coarse mesh over the problem geometry. The boundaries of each coarse mesh are determined by the pin array and various material zones of the problem, as illustrated by the bold outlines in Figure 3.2. Each coarse mesh defines a cell of a various type, where different cell types are distinguished by their

contents. Cylinders are typically centered in a cell, although this is not a requirement and is often modified by the code to account for oversized water rods. Unique cell types have been created to handle pins along the edge of the channel shroud and in each corner of the channel, where the specific intricacies associated with the rounded box wall and the variation in wall thickness on the more modern bundle designs require special attention. Additional cell types have been created to handle the oversized water rods found in the various GE/GNF bundle designs and the water boxes, water diamonds, and water wings found in other popular bundle designs. Still more cell types exist to model the various portions of a control blade, and so on.

Once the Cartesian coarse mesh has been created and the various cells have been defined throughout the lattice, the ray tracing routine proceeds to subdivide each cell into smaller meshes that will define the flat flux regions of the problem. The default meshing for the vanish portion of a GE14 bundle design has been chosen for illustration in Figure 3.2. Mesh sub-divisions in cells that contain embedded cylinders are created at increments of either 22.5° or 45° angles, depending on the detail required for an accurate solution to the problem (larger pins require the finer azimuthal mesh). Note that the azimuthal mesh are used simply to define flat flux regions during the MoC solution and are not used to define azimuthal burnup zones per fuel pellet. An annular mesh is added to the coolant region of each pin cell, as illustrated in Figure 2.4, to help capture the steep thermal flux gradient in the coolant. Volumes are calculated for every mesh in the problem and are used to ratio track lengths at the end of the ray tracing process to ensure conservation during the MoC solution.

Once all mesh volumes have been calculated, the MoC routine is ready to begin ray tracing across the problem. Ray tracing takes place only for the azimuthal directions of motion between $0 \leq \bar{\varphi}_i' \leq \pi$ and only in the xy-plane of the problem. After the ray tracing has been completed, the tracks are raised out of the plane of the problem to each of the various polar angles and the lengths are adjusted accordingly.

A detailed description of ray tracing is included in Reference [10]. The ray tracing consists of determining the intersections of each characteristic with each mesh in the problem. The track lengths are calculated as the distance between successive intersections.

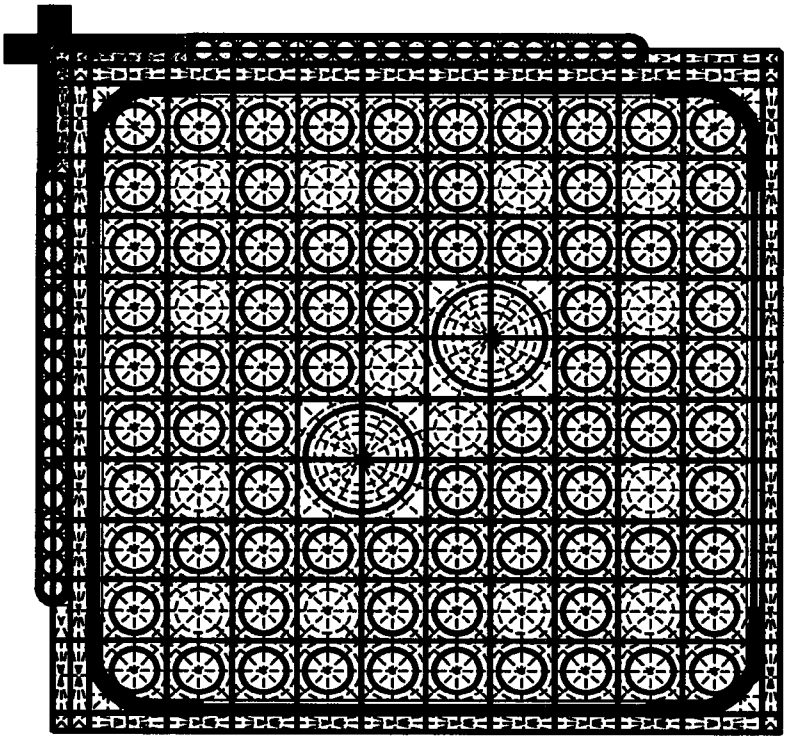

**Figure 3.2 Example of MoC default fine-meshing for the vanish portion of a GE14 fuel design.**

### *3.3. Preserving Mesh Volume*

Once the ray tracing routine has calculated all track lengths in the xy-plane of the problem, the track lengths need to be modified to ensure that the solution to the characteristics equation preserves the volume of each mesh in the problem. For a given number of track segments crossing a mesh, the volume traced by the track segments moving in a specific direction is approximated as,

$$A_{i,n,approx} = \sum_k t_{k,n}(\bar{\varphi}_i') \cdot d_i' \tag{56}$$

where $t_{k,n}(\bar{\varphi}_i')$ is the length of the $k$'th track segment at azimuthal angle $\bar{\varphi}_i'$ in the xy-plane of the problem, crossing mesh $n$; and $d_i'$ is the modified track separation at azimuthal angle $\bar{\varphi}_i'$, obtained from Eq. (54).

Each track segment is modified using the ratio between the true and the approximated volume of the mesh,

$$t'_{k,n}(\bar{\varphi}_i') = t_{k,n}(\bar{\varphi}_i') \cdot \frac{A_{n,true}}{A_{i,n,approx}} = t_{k,n}(\bar{\varphi}_i') \cdot \frac{A_{n,true}}{\sum_k t_{k,n}(\bar{\varphi}_i') \cdot d_i'} \tag{57}$$

The modified track lengths in the xy-plane from Eq. (57) are used in the solution to the characteristics equation.

### *3.4. Solution to the Characteristics Equation*

The equation that we are interested in solving is Eq. (35), rewritten below in a simplified form,

$$\Phi^G_{k,n,out}(\bar{\varphi}_i,\bar{\theta}_j) = \hat{Q}^G_n + \exp\left[-\Sigma^G_{tr,n}\tau_{k,n}(\bar{\varphi}_i,\bar{\theta}_j)\right]\cdot\left(\Phi^G_{k,n,in}(\bar{\varphi}_i,\bar{\theta}_j) - \hat{Q}^G_n\right) \tag{58}$$

where $\tau_{k,n}(\bar{\varphi}_i,\bar{\theta}_j) = t'_{k,n}(\bar{\varphi}')/\sin\bar{\theta}_j$ is the modified track length after being lifted out of the xy-plane of the problem to the appropriate polar angle; and $\hat{Q}^G_n = q^G_n/4\pi\Sigma^G_{tr,n}$ is the term containing the angular source. [[

]] The scalar source term included in Eq. (58) is calculated as,

$$q^G_n = \sum_{G'}\left(\Sigma^{G'\to G}_{s,n} + \frac{\Sigma^{G'\to G}_{p,n}}{k^\infty}\right)\phi^{G'}_n \tag{59}$$

where the production cross section is defined as $\Sigma^{G'\to G}_{p,n} = \chi^G_n \sum_{G'} \nu\Sigma^{G'}_{f,n}$.

The scalar flux in Eq. (59) – for any given mesh – is obtained from Eq. (36),

$$\phi^G_n = \sum_j\sum_i\sum_k \bar{\Phi}^G_{k,n}(\bar{\varphi}_i,\bar{\theta}_j)\cdot\omega_i\cdot\omega_j \tag{60}$$

After substituting the expression for the average angular flux across a mesh into Eq. (60), we obtain the following expression for the scalar flux, where all sources are considered isotropic (using transport-corrected cross sections to account for anisotropic effects),

$$\phi^G_n = \hat{Q}^G_n + \frac{1}{\Sigma^G_{tr,n}}\sum_j\sum_i\sum_k \frac{\Delta^G_{k,n}(\bar{\varphi}_i,\bar{\theta}_j)\cdot\omega_i\cdot\omega_j\cdot\sin\bar{\theta}_j}{t'_{k,n}(\bar{\varphi}_i)} \tag{61}$$

where $\Delta^G_{k,n}(\bar{\varphi}_i,\bar{\theta}_j) = \Phi^G_{k,n,in}(\bar{\varphi}_i,\bar{\theta}_j) - \Phi^G_{k,n,out}(\bar{\varphi}_i,\bar{\theta}_j)$; and $\tau_{k,n}(\bar{\varphi}_i,\bar{\theta}_j)$ has been replaced with $t'_{k,n}(\bar{\varphi}_i)/\sin\bar{\theta}_j$. Substituting Eq. (59) into Eq. (61) we arrive at our final expression for the scalar flux,

$$\phi^G_n = \hat{Q}^G_n + \frac{1}{\Sigma^G_{tr,n}A_{true}}\sum_j\sum_i \omega_{ij}\sum_k \Delta^G_{k,n}(\bar{\varphi}_i,\bar{\theta}_j) \tag{62}$$

where $\omega_{ij} = \omega_i\cdot d'_i\cdot\omega_j\cdot\sin\bar{\theta}_j$.

Equations (58), (59), and (62) constitute the set of equations that need to be solved in order to obtain a solution to the transport equation.

## *3.5. Acceleration*

### 3.5.1. Spatial Acceleration

The scalar flux is accelerated spatially using a simple coarse mesh rebalance (CMR) throughout the system [13],[16]. Coarse meshes are defined at the beginning of the ray tracing routine, as illustrated by bold outlines in Figure 3.2. The balance equation to be solved in each coarse mesh is,

$$\left[\sum_{n\in N}\Sigma^G_{t,n}\phi^G_n V_n + \sum_{s\in N}\psi^G_{s,N,out}A_{s,N}\right]\cdot f^G_N = \sum_{n\in N}q^G_n V_n + \sum_{s\in N}\psi^G_{s,N,in}A_{s,N}\cdot f^G_{N'} \tag{63}$$

where $n$ represents the fine-mesh subdivisions and material regions that make up a coarse mesh, $N$; $s$ represents the surfaces to the coarse mesh; $\psi^G_{s,N,out}$ represents the outward-directed scalar flux along surface $s$ of coarse mesh $N$; $A_{s,N}$ represents the surface area; and $N'$ represents the coarse mesh that shares surface $s$ with coarse mesh $N$.

The integrated surface flux, $\psi^G_{s,N,out}A_{s,N}$ , is accumulated as Eq. (58) is solved. The contribution to the outward-directed integrated angular flux along a coarse mesh surface is calculated as,

$$\psi^G_{s,N,out}A_{s,N} = \sum_j\sum_i \omega_{ij}\sum_k \Phi^G_{k,n,out}(\bar{\varphi}'_i,\bar{\theta}_j) \tag{64}$$

where the summation is only accumulated if $\Phi^G_{k,n,out}(\bar{\varphi}'_i,\bar{\theta}_j)$ is along the edge of coarse mesh $N$. This information is obtained from the ray tracing routine.

Eq. (63) is solved iteratively for the balance factors, $f^g_n$ , using a red-black iteration scheme. Once the balance factors have been determined, the scalar flux is updated,

$$\phi^G_n = \phi^G_n \cdot f^G_N \tag{65}$$

for all mesh subdivisions, $n$, within coarse mesh region $N$. The CMR calculation is performed at the end of each inner iteration.

Since the CMR acceleration scheme can be unstable under certain conditions, the acceleration is applied as long as the total number of outer iterations is below a reasonable level. If the number of outer iterations exceeds this level, the CMR is disengaged and the flux is solved without any spatial acceleration. Such conditions rarely, if ever, exist for typical single-problems common to LWR reactor analysis.

Implementation of the CMR acceleration scheme can usually reduce the total number of outer iterations by a factor of 3 to 4, depending on the type of problem being analyzed. It should be mentioned that there usually exists an excellent flux guess from a previous state point from which to start each calculation. Because of this, no more than a dozen outer iterations are often needed to fully converge the flux, so the acceleration scheme is of minimal importance.

### 3.5.2. Energy Acceleration

Following completion of an outer iteration, a fundamental mode rebalancing of the group flux distribution is performed in order to properly normalize the flux and ensure neutron conservation. The fundamental mode calculation is performed on an equivalent homogeneous system using flux- and volume-weighted cross sections from the heterogeneous calculation, as in Eq. (38). The fundamental mode equation to be solved is,

$$\bar{\phi}_{FM}^{G} = \bar{q}^{G} / \bar{\Sigma}_{r}^{G} \tag{66}$$

where the source term does not include self scattering and the removal cross section is defined as in Eq. (41). The source term is calculated as $\bar{q}^{G} = \sum_{G' \neq G} \bar{\Sigma}_{s}^{G' \to G} \bar{\phi}_{FM}^{G'} + \bar{\chi}^{G}$ and the corresponding eigenvalue to the system is calculated as $k^{\infty} = \sum_{G'} \nu \bar{\Sigma}_{f}^{G'} \bar{\phi}_{FM}^{G'}$, where the flux has been normalized such that there is one neutron being absorbed in the system.

Due to upscattering in the thermal energy groups, the solution to Eq. (66) defines an iterative process and the fundamental mode equation is solved directly, with no acceleration. Following the solution to Eq. (66), the scalar flux distribution from Eq. (65) is scaled using the rebalance factors,

$$\hat{\phi}_{n}^{G} = \phi_{n}^{G} \cdot \frac{\bar{\phi}_{FM}^{G}}{\sum_{n} \phi_{n}^{G} V_{n}} \tag{67}$$

where the summation in the denominator of Eq. (67) is over all mesh in the problem.

The fundamental mode rebalance calculation in LANCR02 can reduce the number of outer iterations needed to converge the flux by about a factor of 2.

## *3.6. Convergence*

This section describes the convergence criteria used in the LANCR02 solution scheme.

### 3.6.1. Convergence of the Angular Flux

For each energy group, $G$, we have an initial value for the inward-directed angular flux along the surface of the problem, in azimuthal direction $\bar{\varphi}_{i}'$, polar direction $\bar{\theta}_{j}$, along track $k$, which is denoted by $\Phi_{k,in}^{G}(\bar{\varphi}_{i}', \bar{\theta}_{j})$. We march along the track until we reach another boundary

to the system, at which point we have an outward-directed angular flux, $\Phi^G_{k,out}(\bar{\varphi}_i', \bar{\theta}_j)$. This, then, becomes the value for the inward-directed angular flux in the reflected (or periodic) direction, $\Phi^G_{k',in}(\bar{\varphi}_{i'}', \bar{\theta}_j) = \Phi^G_{k,out}(\bar{\varphi}_i', \bar{\theta}_j)$. The new value replaces the previous value for the inward-directed angular flux in the reflected direction $(\bar{\varphi}_{i'}', \bar{\theta}_j')$. The difference between the two values – the value of the inward-directed boundary angular flux at the end of the previous iteration, and the value at the end of the present iteration – will approach zero as the solution converges. When all inward-directed boundary angular flux values have changed by less than a certain criterion, ε, from their values at the end of the previous iteration, the angular flux for that particular energy group is assumed to be converged,

$$\left| \frac{\Phi^G_{k,in}(\bar{\varphi}_i', \bar{\theta}_j)\big|_{new} - \Phi^G_{k,in}(\bar{\varphi}_i', \bar{\theta}_j)\big|_{old}}{\Phi^G_{k,in}(\bar{\varphi}_i', \bar{\theta}_j)\big|_{old}} \right| < \varepsilon \tag{68}$$

In LANCR02, Eq. (68) must hold true for all *i*'s, *j*'s, and *k*'s in all energy groups in order to satisfy a fully converged solution to the problem.

### 3.6.2. Convergence of the Scalar Flux

At the end of each inner iteration, in addition to testing for convergence of the inward-directed boundary angular flux, the scalar flux is also tested for convergence. The same principle applies here as for the angular flux. We begin the iteration with some value for the scalar flux in group *G*, $\phi^G_n\big|_{old}$. This value is used to calculate the source term before solving for the new flux distribution. With the source distribution frozen in group *G*, we solve for a new scalar flux distribution, $\phi^G_n\big|_{new}$. The difference between the old and new value of the scalar flux will approach zero as the solution converges. As in the case of the angular flux, convergence in LANCR02 is declared when the following statement is satisfied in every mesh, every energy group,

$$\left| \frac{\phi^G_n\big|_{new} - \phi^G_n\big|_{old}}{\phi^G_n\big|_{old}} \right| < \varepsilon \tag{69}$$

### 3.6.3. Convergence of the Eigenvalue

Before starting an outer iteration, the eigenvalue for the old flux distribution is calculated, $k^\infty$. As the fission source distribution converges, so too will the eigenvalue. From one iteration to the next, LANCR02 checks for convergence of the eigenvalue,

$$\left| \frac{k^\infty\big|_{new} - k^\infty\big|_{old}}{k^\infty\big|_{old}} \right| < \varepsilon \tag{70}$$

Eq. (70) will always be satisfied if both Eqs. (68) and (69) are satisfied. That is, the eigenvalue will always be converged if the flux distribution is converged. For this reason, satisfying Eq. (70) is relatively irrelevant.

By default, LANCR02 sets the value of $\varepsilon$ to $10^{-5}$ in Eqs. (68),(69), and (70). The MoC module in LANCR02 is single precision.

# 4. Power Distribution Calculation

## *4.1. Overview*

The power generated in a fuel rod is the sum of energy from gamma and beta decay, as well as kinetic energy from fission. The various contributions to the power are calculated as;

#### *4.1.1.1. Kinetic energy of fission fragments and neutrons in fuel rod* I*:*

$$E_{kinetic,I} = \sum_{iso} q'_{fission,iso} \sum_{i \in I} \sum_{G} N_{iso,i} \sigma^{G}_{f,iso,i} \phi^{G}_{i} V_{i} \tag{71}$$

where

$q'_{fission,iso}$ = kinetic energy of fission fragments and neutrons from fission of nuclide *iso*

#### *4.1.1.2. Total gamma energy deposited in fuel rod* I*:*

$$E_{\gamma,I} = \sum_{i \in I} \sum_{\gamma} \Sigma^{\gamma}_{e,i} V_{i} \phi^{\gamma}_{i} \tag{72}$$

#### *4.1.1.3. Beta energy due to absorption in fuel rod* I*:*

$$E_{\beta,I} = \sum_{iso} q'_{\beta,iso} \sum_{i \in I} \sum_{G} N_{iso,i} \sigma^{G}_{a,iso,i} \phi^{G}_{i} V_{i} \tag{73}$$

#### *4.1.1.4. Loss of kinetic energy due to fast neutron capture in fuel rod I :*

$$E_{c,I} = \sum_{iso} \sum_{i \in I} \sum_{G>5.53keV} q'^{G}_{iso,i} N_{iso,i} \sigma^{G}_{c,iso,i} \phi^{G}_{i} V_{i} \tag{74}$$

where

$q'_{c,iso}$ =loss of neutron kinetic energy due to $G$ th group neutron capture

[[

]]

# 5. Burnup Model

## *5.1. Various Types of Burnup Calculations*

Three types of burnup calculations are provided in LANCR02: (1) a fuel burnup calculation; (2) a control blade burnup calculation – with or without fuel depletion; and (3) a shutdown cooling calculation.

### 5.1.1. Fuel Burnup

The fuel burnup calculation is used for typical fuel/core design calculations. Any pellet can be sub-divided into multiple material zones of equal volume. Each material zone is modeled using a unique set of number densities. [[

]]

### 5.1.2. Control Blade Depletion

The control blade depletion calculation without bundle depletion is used for control blade life-time evaluations. Control blade depletion calculation together with fuel burnup is also possible. Absorber rods may be sub-divided annularly into individual material regions or modeled whole. Each absorber rod in a control blade wing may be its own unique depletion region or any number of rods may be grouped together and depleted as an average.

### 5.1.3. Cooling Calculation

The cooling calculation is engaged if the cooling option is selected and time after shutdown is greater than 0.0. Through the cooling calculation, short-lived nuclides are depleted before entering the neutron transport calculation. Alternatively, the user may use no Xenon option, which sets all $I^{135}$ and $Xe^{135}$ number densities to zero, simulating a shut down period of a few days. This option does not simulate the build-up of $Sm^{149}$ following shut down.

## *5.2. Burnup Calculation*

### 5.2.1. Equations to be Solved

The burnup chains contained in LANCR02 are diagrammed in Figure 5.1 through Figure 5.5. The burnup equation to be solved in LANCR02 is the first-order differential equation of the type,

$$\frac{dN_{iso}}{dt} = \sum_{iso'} u_{iso,iso'}\lambda_{iso'}N_{iso'} + \sum_{iso'} v_{iso,iso'}(\sum_g \sigma^g_{c,iso'}\phi^{\prime g})N_{iso'} + \sum_{iso'} w_{iso,iso'}(\sum_g \sigma^g_{(n,2n),iso'}\phi^{\prime g})N_{iso'}$$
$$+\sum_{iso'} \gamma_{iso,iso'}(\sum_g \sigma^g_{f,iso'}\phi^{\prime g})N_{iso'} - \left\{\lambda_{iso} + (\sum_g \sigma^g_{a,iso}\phi^{\prime g}) + (\sum_g \sigma^g_{(n,2n),iso}\phi^{\prime g})\right\}\cdot N_{iso} \quad (75)$$

where $u_{iso,iso'}$, $v_{iso,iso'}$, $w_{iso,iso'}$ are branching ratios for decay, neutron capture, and (n,2n) reactions, respectively; $\lambda_{iso}$ is the decay constant for isotope *iso*; $\gamma_{iso,iso'}$ is the fission yield; and $\phi^{\prime g}$ is the flux distribution from the leakage-corrected flux from the MoC solution. Eq. (75) has a solution of the form,

$$N_{iso}(\Delta t) - N_{iso}(0) = (Q - \tilde{\lambda}_{iso}N_{iso}(0))\ \frac{(1-e^{-\tilde{\lambda}_{iso}\cdot\Delta t})}{\tilde{\lambda}_{iso}} \quad (76)$$

where the effective decay constant, $\tilde{\lambda}_{iso}$, is equal to $\tilde{\lambda}_{iso} = \lambda_{iso} + (\sum_g \sigma^g_{a,iso}\phi^{\prime g}) + (\sum_g \sigma^g_{n2n,iso}\phi^{\prime g})$ and the production term, $Q$, is assumed constant over a small time interval, $\Delta t$.

The solution to Eq. (75) is obtained using a 4th order Runge-Kutta-Gill algorithm for the predictor step. For the corrector step, the effective decay constant is assumed to vary linearly over the time step, Δt, and

$$\frac{dN_{iso}}{dt} = -(\lambda_0 + \lambda_1 t)N_{iso} + \bar{Q} \quad (77)$$

where $\lambda_0$, $\lambda_1$, and $\bar{Q}$ are obtained from the solution during the predictor step. The corrector step solves for the analytic solution explicitly,

$$N(t) = N(0)e^{-\bar{\lambda}\cdot t} + 2a\cdot\frac{\bar{Q}}{\lambda_0}\cdot\left[F(b) - e^{-\bar{\lambda}\cdot t}F(a)\right]$$

$$a = \frac{\lambda_0}{\sqrt{2\lambda_1}} \quad b = \frac{\lambda_0 + \lambda_1 t}{\sqrt{2\lambda_1}} \quad (78)$$

where $\bar{\lambda}$ is the average decay constant from the predictor solution; and *F(x)* is a Dawson's integral,

$$F(x) = e^{-x^2}\int_0^x e^{u^2}du \quad (79)$$

Solution to Eq. (78) supplies the final number densities at the end of the time step.

### 5.2.2. Dual Time Step Model

For fuel mixtures that contain $UO_2$ or MOX isotopes, depletion step sizes as large as 2 GWd/ST (GWd/ST = Gigawatt day per short ton) are sufficient to accurately deplete the heavy metal and build in the higher actinides and fission products. For fuel mixtures that contain gadolinium, however, a time step size of 2 GWd/ST can introduce large errors into the results from the lattice physics code. This sensitivity is caused by the large spatial self-shielding of the $Gd^{155}$ and $Gd^{157}$ isotopes that create rapid changes in the thermal flux distribution across the fuel pellet as the gadolinium depletes. To accurately capture the depletion rate of the gadolinium, time step sizes on the order of 0.2 GWd/ST are typically required at the lattice level.

To account for the different depletion rates of the various isotopes, dual time steps in LANCR02 are used to handle lattice designs that contain fuel pins with gadolinium. The complete series of 1-D pin cell calculations, followed by the 2-D RM calculation and 2-D MoC calculation, are performed at lattice depletion time step increments of 1 GWd/ST. In between complete lattice calculations, gadolinium pins are depleted at 0.2 GWd/ST time step increments by re-performing only the 1-D pin cell calculations and using the flux distribution from the previous RM and MoC calculations to augment the updated pin cell flux.

We can express our depletion scheme by re-stating Eqs. (32), (42), (43) and with the updated pin cell flux, $\psi_i^g$,

$$\tilde{\psi}_i^g = \psi_i^g \cdot \frac{\phi_I^g V_I}{\sum_{i \in I} \psi_i^g V_i} \tag{80}$$

$$\psi_i'^g = \tilde{\psi}_i^g \cdot \frac{\phi_i^G}{\sum_{g \in G} \tilde{\phi}_i^g} \tag{81}$$

$$\psi_i''^g = \psi_i'^g \cdot \frac{\Psi^g \cdot \sum_i V_i}{\sum_{i \in I} \psi_i'^g V_i} \tag{82}$$

where $\phi_I^g$ is the fine-group flux from the most recent RM calculation; $\tilde{\phi}_i^g$ is the most recent fine-group condensation flux; $\phi_i^G$ is the transport-group flux from the most recent MoC calculation; and $\Psi^g$ is the fine-group critical flux from the most recent fundamental mode calculation.

The dual time steps continue until the $Gd^{155}$ and $Gd^{157}$ isotopes have been sufficiently depleted from all pins, at which time the code reverts to standard default time steps of 2 GWd/ST.

### 5.2.3. Choice of Time Step

LANCR02 provides three types of time step input: MWd/MT, day, and MWd/ST. Time intervals are converted from exposure to day using the relation,

$$\Delta t = \frac{\Delta E \cdot FNA}{const \cdot P_0} \tag{83}$$

where $\Delta t$ is the time interval in days; $\Delta E$ is the exposure step size in either MWd/MT or MWd/ST; $P_0$ is the power density in W/cm$^3$; *const* is a constant equal to either 0.602472 for MWd/MT or 0.546576 for MWd/ST; and *FNA* is the initial density of heavy metal in g/cm$^3$.

## *5.3. Fissile and Fertile Chain*

The fissile and fertile chain diagram is shown in Figure 5.1.

## *5.4. Fission Product Chain*

The fission product (FP) chain contains two pseudo FPs that are used as collection bins at the end of several sub-chains. The pseudo FPs have no cross sections associated with their number densities. The FP chain diagrams are illustrated in Figure 5.2 through Figure 5.4.

## *5.5. Burnable Absorber Chain for Control Blade Isotopes*

Two elements used as absorber material in control blades can be modeled as time-dependent in LANCR02. The $B^{10}$ and Hf depletion chains are represented in Figure 5.5.

[[

]]

**Figure 5.1 Fissile and fertile chain diagram**

[[

]]

**Figure 5.2 FP chain diagram (1 of 3)**

[[

]]

**Figure 5.3 FP chain diagram (2 of 3)**

[[

]]

**Figure 5.4 FP chain diagram (3 of 3)**

[[

]]

**Figure 5.5 Boron and Hafnium chain diagram**

# 6. VOID DISTRIBUTION

## *6.1. Overview*

LANCR02 is capable of superimposing a non-uniform void distribution across the in-channel flow area of the lattice. The impact from the option is most visible over the range of void fraction levels from 0.25 to 0.55. Obviously, at 0.0 void and 1.0 void there is nothing to be distributed.

The non-uniform void model re-distributes the void to the high energy regions of the lattice. Consequently, the non-uniform void option will result in an increase in control rod worth, a more rapid depletion rate of the gadolinium isotopes, and a reduction in pin peaking factors.

## *6.2. Power Distribution Calculation*

In order to implement the distributed void model non-uniform void model, a pin-wise power distribution is required. [[

]]

## *6.3. Void Distribution Model*

[[

]]

**Table 6.1 Void Distribution Model Control Blade Corrections**

| | | |
|---|---|---|
| [[ | | |
| | | |
| | | |
| | | |
| | | |
| | | |
| | | ]] |

[[

]]

[[ ]]

[[

]]

[[

]]

[[

]]

[[

]]

[[

]]

[[

]]

[[

]]

# 7. CONTROL BLADE DEPLETION MODEL

## *7.1. Introduction*

LANCR02 allows users to insert a control blade into the NW corner of the lattice for any calculation that contains an outer water gap. By default, the absorber isotopes in the control blade are not depleted, even if the problem being analyzed is a depletion case. The user can, however, instruct the code to deplete the absorber isotopes in the control blade. The user may choose to deplete the absorber isotopes in the control blade together with the burnable isotopes in the fuel pellets, or may choose to deplete the absorber isotopes in the control blade (c/b) without depleting the burnable isotopes in the fuel pellets.

## *7.2. Creating Depletion Zones*

Any number of depletion zones may be created in the control blade. The user specifies depletion zones using an array in the input deck. A depletion zone is assigned to each absorber rod in the control blade along with the number of absorber rods in the c/b. This is illustrated in Figure 7.1.

Isotopics are averaged for each absorber zone. [[

]]

## *7.3. Annular Depletion Rings*

[[

]]

## *7.4. Depletion Mode*

As described earlier in this section, LANCR02 allows for two different modes of control blade depletion: (1) the c/b absorber rods deplete without depleting the burnable isotopes in the fuel pellets or (2) the c/b absorber rods deplete while also depleting the burnable isotopes in each fuel pellet.

The first mode of c/b depletion is most useful for determining the lost worth of the blade over the control blade's lifetime. Since the fuel is not allowed to deplete, the reactivity of the bundle is frozen during the burnup step and the change in reactivity from beginning-of-life (BOL) value is due entirely to the depletion of the absorber isotopes in the control blade. Time steps are based on the power generated by isotopes present in the fuel at BOL.

The second mode of c/b depletion is a more realistic representation of how the absorber isotopes would deplete together with the burnable isotopes in the fuel pellets.

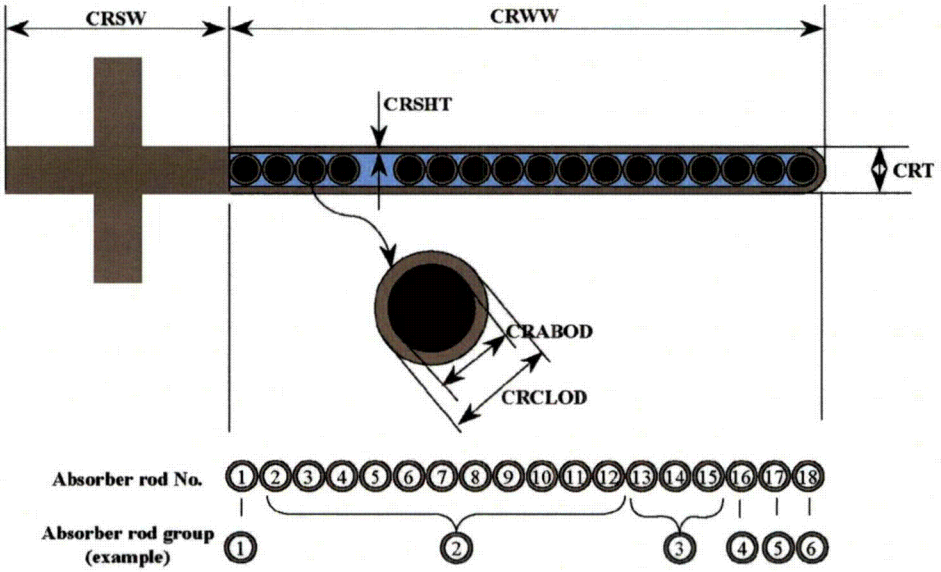


**Figure 7.1 Variables related to a pin type control blade model.**

**Table 7.1 Variables related to control blade geometry.**

| Legend | Description |
|---|---|
| ICRX | Cruciform control blade type |
| CRT | Control blade thickness |
| CRSW | Control blade center support length |
| CRWW | Control wing length |
| CRSHT | Control blade sheath thickness |
| CRCLOD | Absorber tube outer diameter |
| CRABOD | Absorber region outer |

# 8. BUNDLE GEOMETRIES

## *8.1. Modeling Various Lattice and Assembly Geometries*

LANCR02 treats a single pin cell, a square array of nxn fuel-rods with or without vanished rods, and various types of fuel assemblies, as listed in Table 8.1 and illustrated in Figure 8.1 through Figure 8.5. The single pin cell and the square array of fuel rods can be characterized as a system, with neither water gaps nor a channel box present. All configurations except the water diamond configuration are treated explicitly, with no significant geometry approximations. The water diamond is approximated by modeling a water box.

**Table 8.1 Standard Geometry Configurations Treated**

| Lattice | | Remarks |
|---|---|---|
| Single fuel rod cell | | Figure 8.1 |
| Square array of fuel rods | | Figure 8.2 |
| GNF/GE fuel assembly | 8x8 | Figure 8.3 |
| | 9x9 | |
| | 10x10 | |
| Water Box | 9x9 | With central water box |
| | 9x9 | With offset water box |
| | 10x10 | Figure 8.4 |
| Water Diamond and Water Cross | 8x8 | No central water diamond |
| | 10x10 | No central water diamond |
| | 10x10 | Figure 8.5 |

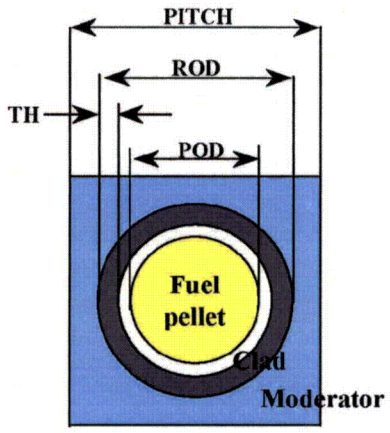


**Figure 8.1 Single pin cell**

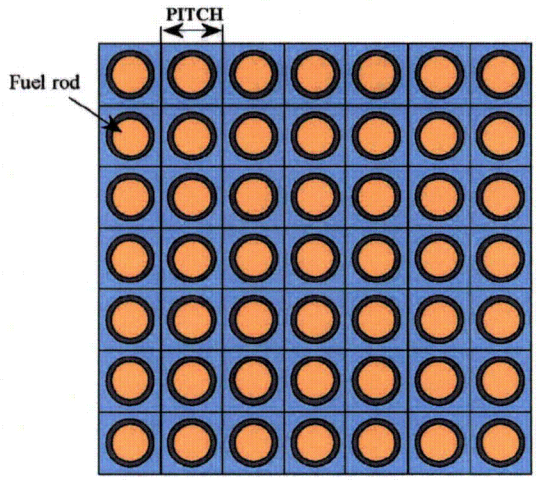


**Figure 8.2 Square array of rods.**

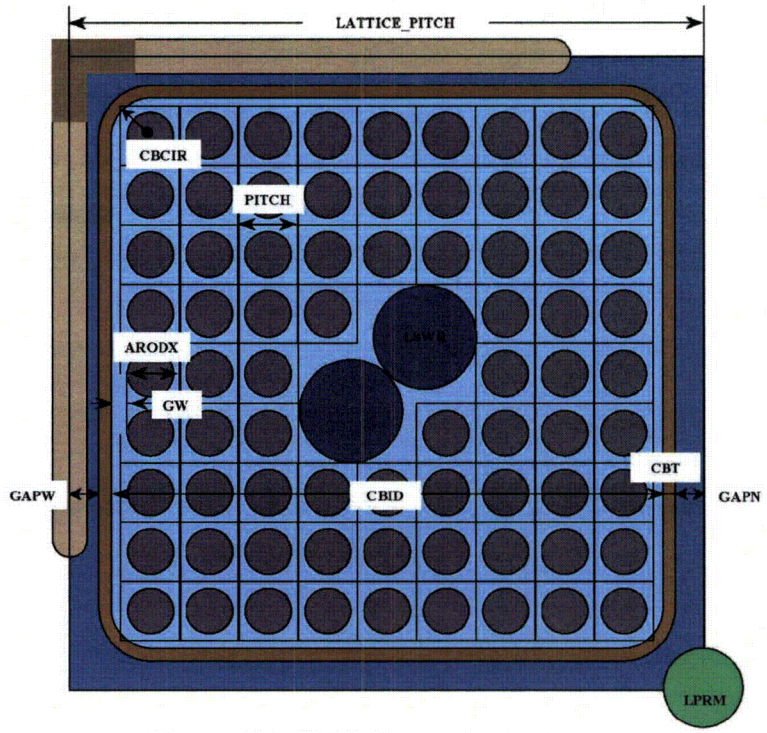


**Figure 8.3 GE 9x9 bundle design.**

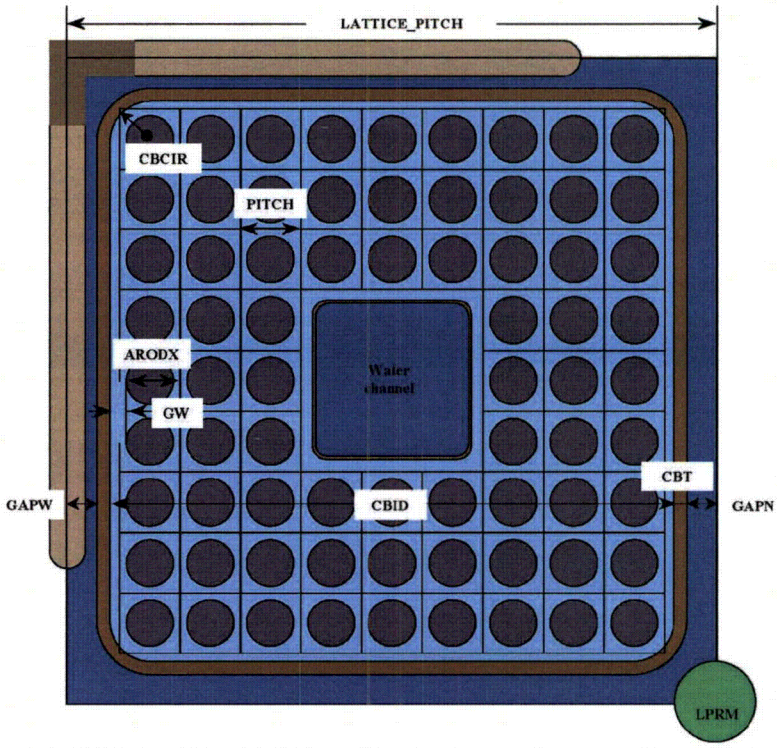


**Figure 8.4 Water Box 9x9 bundle design with central water box.**

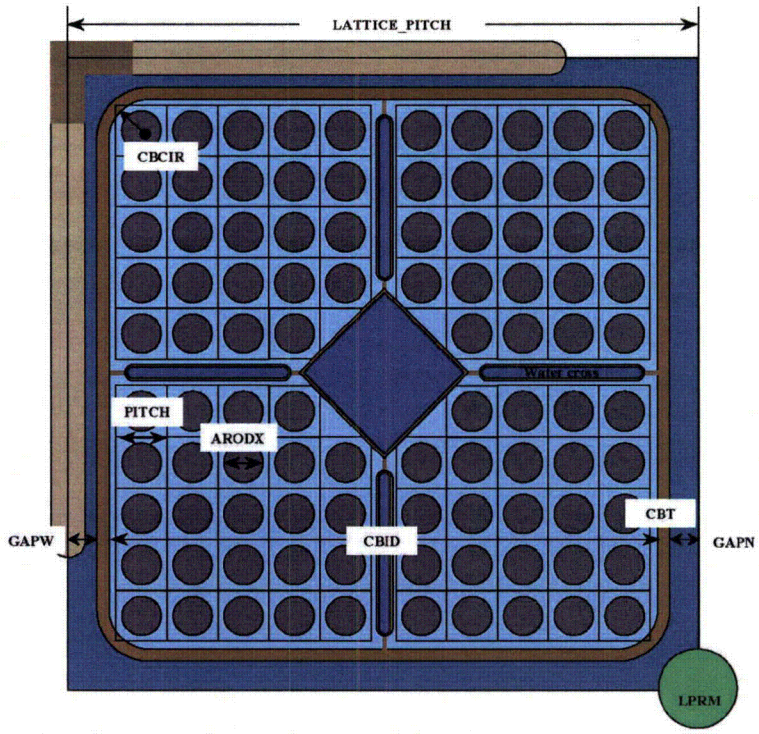


**Figure 8.5 Water Cross bundle design with central water diamond.**

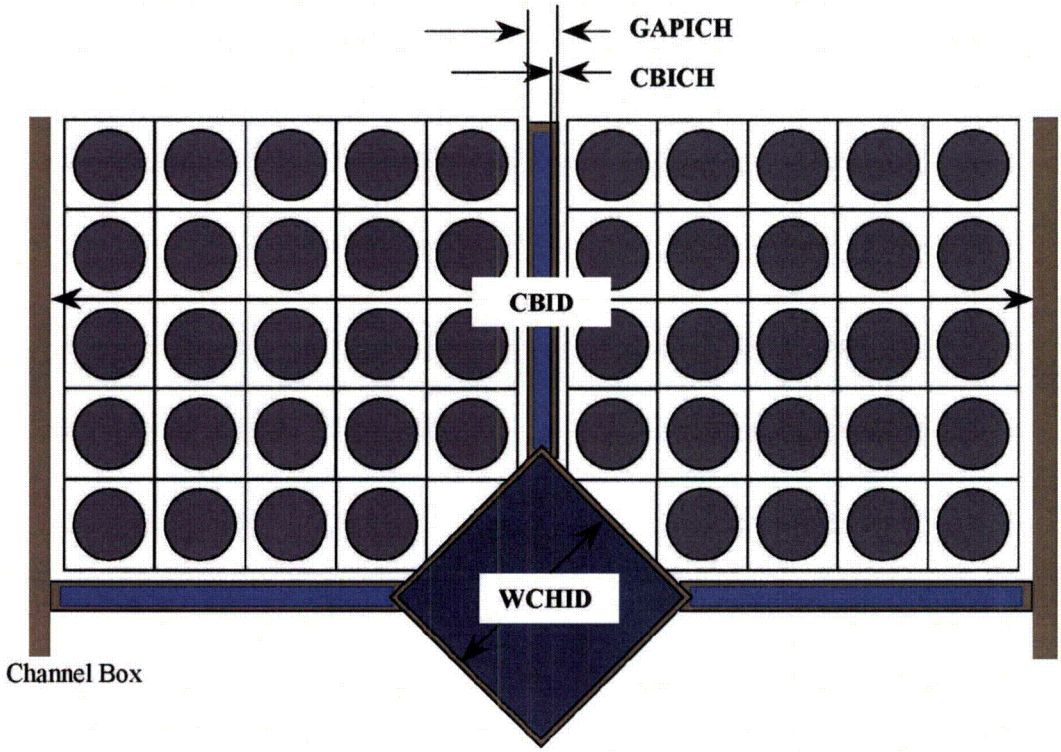


**Figure 8.6 Variables related to the water wing and central water diamond.**

**Table 8.2 Variables Related to Lattice Geometry Definition**

| Legend | Explanation |
|---|---|
| PITCH | Fuel rod pitch |
| GAPW | W-W outer gap half-width |
| GAPN | N-N outer gap half-width |
| GAPWE | Half-width of west side outer water gap |
| GAPSO | Half-width of south side outer water gap |
| GAPEA | Half-width of east side outer water gap |
| GAPNO | Half-width of north side outer water gap |
| | |
| CBID | Channel box inside width |
| CBT | Channel box thickness (thickest part) |
| CBCIR | Channel box corner inside radius |
| CWRL | Width of connection part between CBT and CBTM |
| CBTM | Channel box thickness (second thickest part) |
| CBML | Width of channel box thickness CBTM left |
| CWRR | Width of connection part between CBTM and CBTT |
| CBTT | Channel box thickness (thinnest part) |
| CBW | Width of channel box thickness CBTT |
| CBMR | Width of channel box thickness CBTM right |
| GWC | Wide-gap side spacing between channel box and fuel rods |
| | |
| NICH | Presence of the water wings (0/1 = no/yes). |
| GAPICH(i) | Total thickness of water wing channel |
| CBICH | Wall thickness of water wing |
| WCHID | Inside width of central water diamond |

## *8.2. Modeling Various Channel Geometries*

Channels of uniform thickness are modeled precisely by the code, including the rounded box corners. Channels of non-uniform thickness – so-called thick-thin channels – are modeled precisely if CBTT is zero. That is, thick-thin channels are modeled precisely if the channel does not contain a side notch. For channels that contain side notches, the thin width of the channel is modified to preserve the total volume of the channel material and then CBTT is set to zero internally in the code. The various channel geometries treated by LANCR02 are illustrated in Figure 8.7 and Figure 8.8.

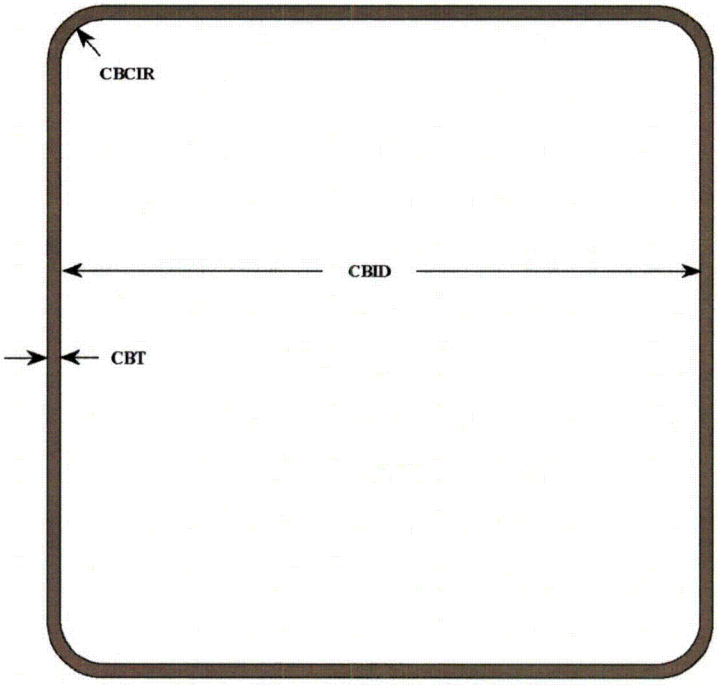


**Figure 8.7 Variables related to a channel of uniform thickness.**

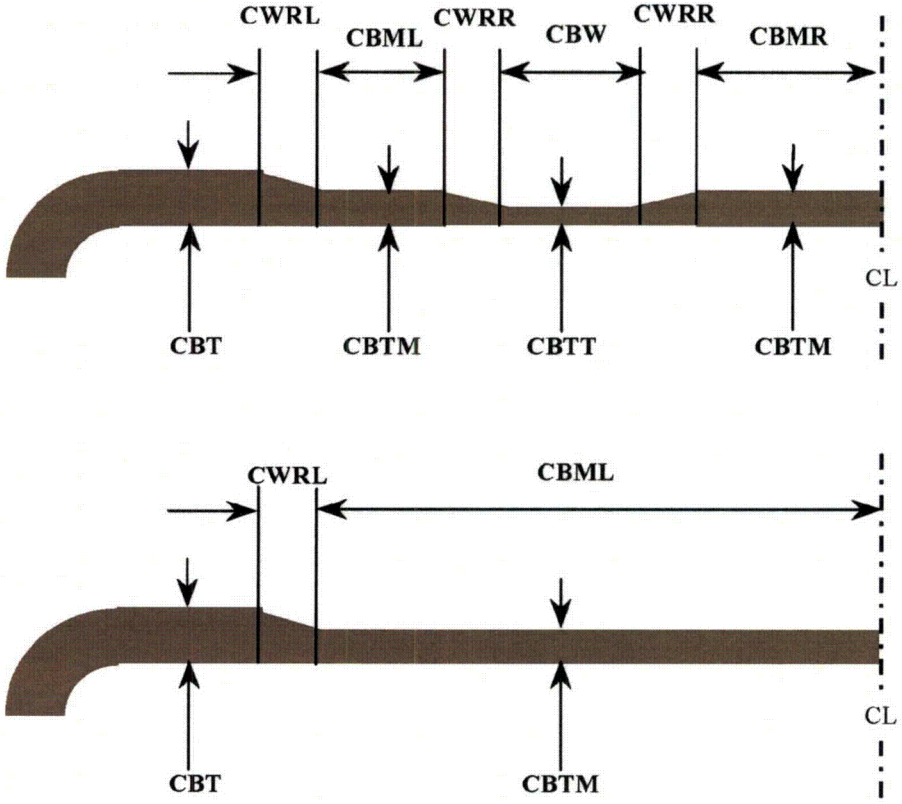


**Figure 8.8 Variables related to a channel of non-uniform thickness.**

## *8.3. Modeling Various Control Blade Geometries*

LANCR02 treats several types of control blades, as listed in Table 8.3.

**Table 8.3 Standard Control Blade Geometries Treated.**

| Type | Calculation model |
|---|---|
| Conventional $B_4C$ Blade | Pin type model |
| Hitachi Hf Rod Control Blade | |
| $B_4C$-Hf Hybrid Control Blade | |
| Marathon Control Blade | |
| ABB Control Blade | |
| Grey-nose Control Blade | Plate type models |
| Toshiba Hf Plate Control Blade | |
| ABWR Hf Flat Tube Control Blade | |

Variables related to the control blade are contained in Table 7.1. The composition of the absorber material is specified via input, which allows the user control over the fraction of $B^{10}$ in the $B_4C$ mixture.

### 8.3.1. Pin type model

All blades that contain absorber rods, tubes, or holes are modeled using the pin type model. The conventional $B_4C$ control blade is modeled as illustrated in Figure 7.1. Each absorber tube in a wing of the blade can be modeled individually, or a single tube can be defined and repeated within the wing. The rounded end of the wing sheath is modeled explicitly by the code. The code also allows for the presence of a central stiffener and models the geometry of the stiffener precisely.

The Hitachi Hf control blade consists of Hf metal rods without cladding. [[

]]

A $B_4C$-Hf hybrid control blade has two types of absorber materials – $B_4C$ rods contained in stainless steel cladding, and a Hf metal bar without cladding. [[

]]

A Marathon control blade can consists of $B_4C$ capsules, Hf absorber rods, and/or empty tubes, all of which are welded to each other to form a wing, as illustrated in Figure 8.9. This blade contains no sheath, but can be modeled similar to the original equipment control blade. [[

]]

A control blade with horizontal absorber holes drilled into a stainless steel wing slab is illustrated in Figure 8.10. [[

]]

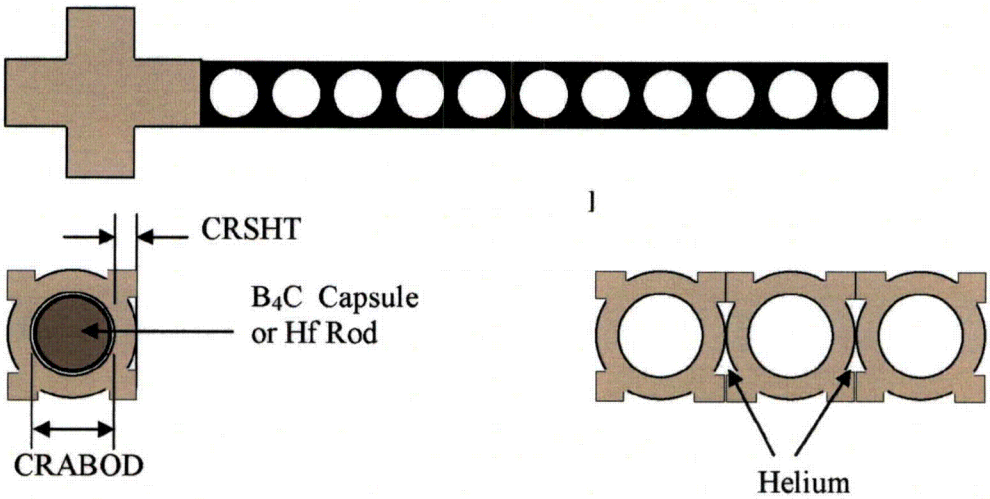


**Figure 8.9 Absorber cells of a Marathon control blade.**

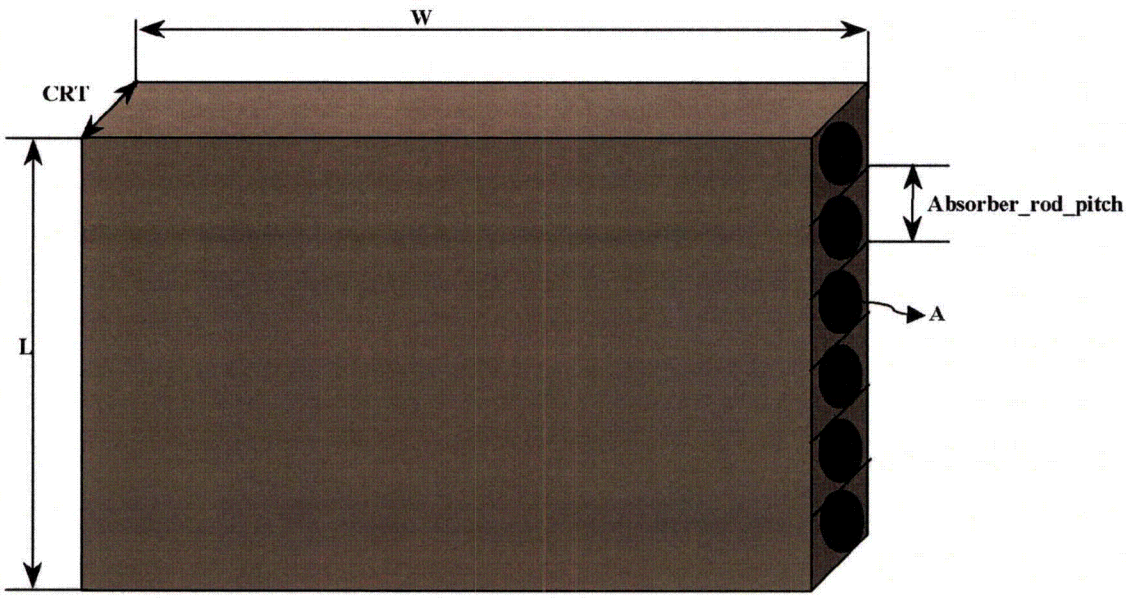


**Figure 8.10 Wing of a control blade with horizontal absorber holes.**

### 8.3.2. Plate type model

Plate type control blades, such as a Toshiba Hf plate control blade, are modeled as illustrated in Figure 8.11. [[

]]

[[

]]

[[

]]

[[

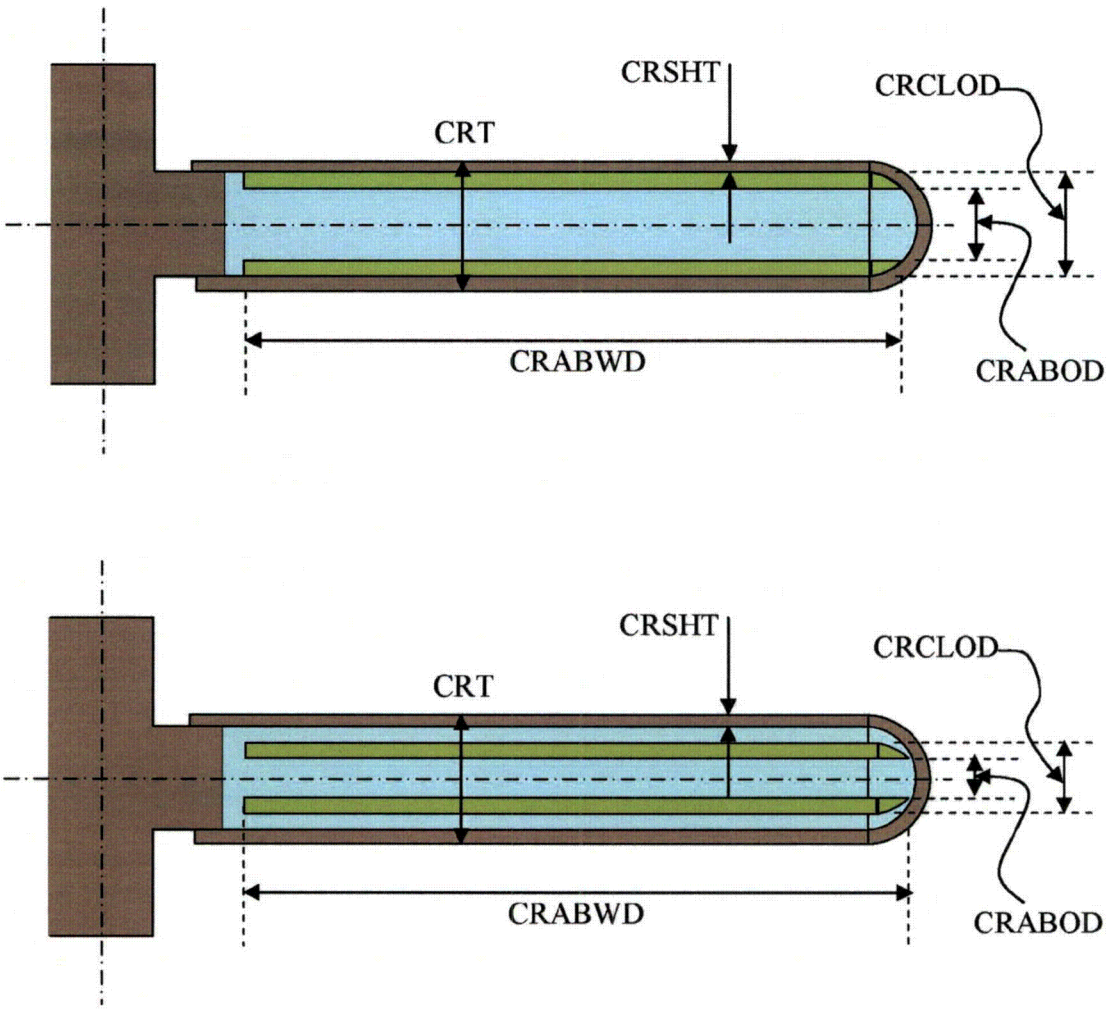


[3]]]

**Figure 8.11 Plate type control blade model (Toshiba Hf plate).**

[[

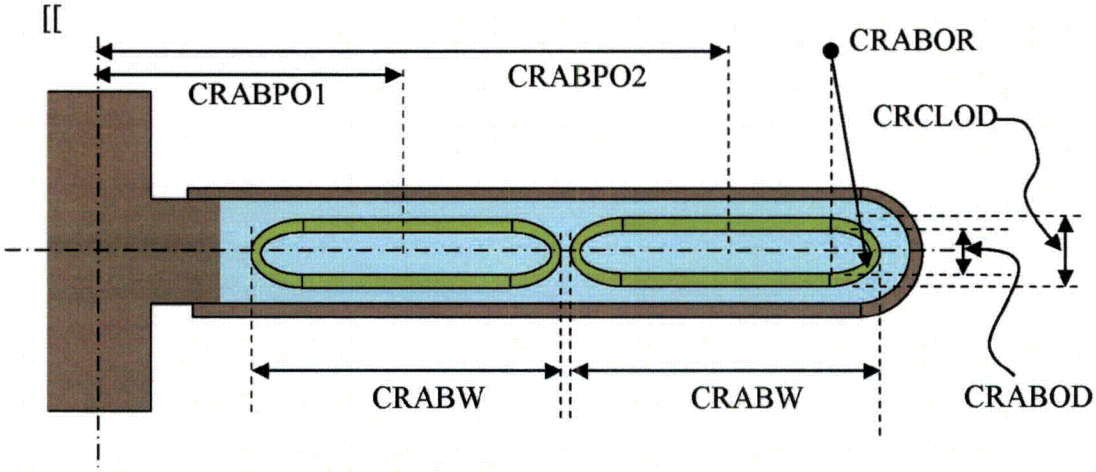


]]

**Figure 8.12 Flat tube type control blade model (Hitachi Hf flat tube)**

## *8.4. Modeling Various Rod Geometries*

LANCR02 models fuel rods and non-fuel cells separately. Each category offers the user several options to model both cell types in true geometry, with the exception of the water diamond model as mentioned in Section 8.1.

### 8.4.1. Fuel Rod Cell

There are 3 different types of fuel rods that can be specified by the user: (1) $UO_2$ fuel rod; (2) MOX fuel rod; and (3) $UO_2$ fuel rod containing burnable absorber. [[

]]

### 8.4.2. Non-Fuel Cell

There are seven separate non-fuel cells that can be modeled: (1) vanish cell containing only coolant; (2) plenum rod containing spring material ; (3) water rod occupying a single pin cell location; (4) oversized water rod occupying 4 pin cell locations; (5) oversized water rod occupying 3.5 pin cell locations (i.e., two rods occupying 7 pin cell locations); (6) oversized water box occupying 9 pin cell locations; and (7) oversized water diamond occupying 4 pin cell locations.

## *8.5. Modeling the BWR Instrument Assembly Geometry*

[[

]]

The instrument assembly model is illustrated in Figure 8.14. In LANCR02, the instrument assembly consists of only 3 regions: (1) the outer cover tube; (2) the insulation region of the tube; and (3) the central anode/cathode region of the sensor.

[[

]]

[[

]]

[[

]]

[[

]]

II

II

**Figure 8.13 Phantom Instrument Assembly Model.**

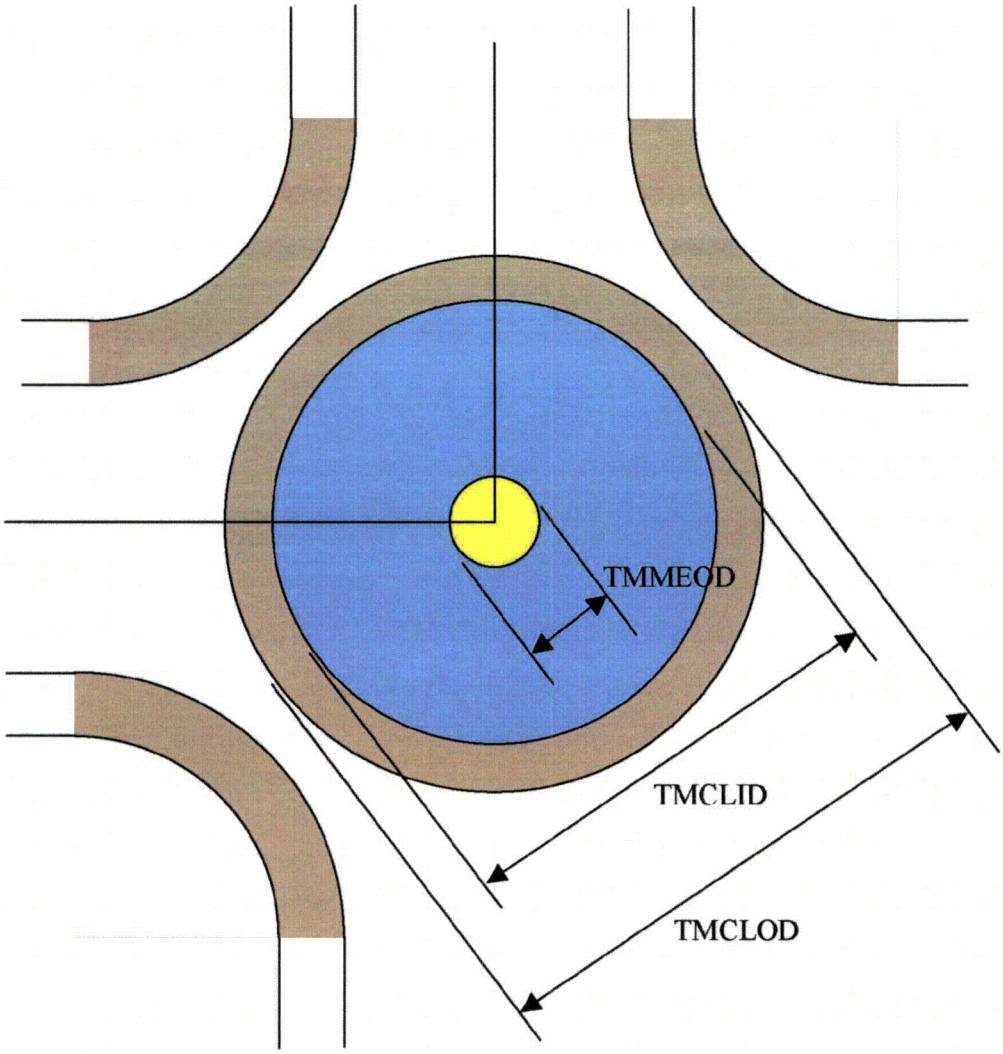


**Figure 8.14 Explicit Instrument Assembly Model.**

# 9. Output

LANCR02 produces output to five separate files. There are three ASCII output files that summarize results such as eigenvalue, pin-wise fission and power distributions, and lattice-averaged isotopic inventories. The ASCII files include: (1) an output file designated .out; (2) a summary file designated .sum; and (3) an error file designated .err that is written only if the code aborts execution. There are two binary data files that may be written to by the code. There is a CEDAR wrap-up file that contains all data necessary to perform a branch calculation, and there is a second binary file that contains data that is to be transferred to the core simulator.

## *9.1. ASCII Output Edit*

The following quantities are edited to the ASCII output file.

- Time : core operation period (days)
- Exposure : lattice-averaged exposure (MWd/t)
- Assembly average few group macroscopic cross sections
- Few group dependent assembly discontinuity factors
- Few group dependent assembly-corner discontinuity factors
- Lattice-averaged isotope-wise neutron balance tables
- Rod-by-rod relative fission distribution and its peaking factor
- Rod-by-rod relative power distribution and its peaking factor
- Rod-by-rod relative exposure distribution and its peaking factor
- Rod-by-rod gamma energy deposition distribution
- Kinetics parameters including effective delayed neutron fraction, prompt neutron life time.
- Effective MeV/fission
- Average fission yields and microscopic capture cross sections for several important FPs, and so on.
- Summary table of k-infinity's and local peaking factors

## *9.2. Binary Output*

The following data are stored in the binary file.

**Nomenclature**

| | |
|---|---|
| $g$ | = few-group energy structure |
| $r$ | = material region (e.g., fuel, clad, coolant, etc.) |
| $s$ | = surface of the assembly |
| $h$ | = 6-group delayed neutron structure |
| $i$ | = fine-group energy structure |
| $j$ | = gamma source group structure |
| $dr = V(r)$ | = volume of material region r |
| $V_{ass}$ | = volume of fuel assembly |

$V_{fuel}$ = total volume of all fuel pellets

$m_{iso}$ =order of nuclide *iso* in the nuclide library

$N_{iso}(r)$ = atomic number density for nuclide *iso*; at position *r*

$A_{iso}$ = atomic mass of nuclide *iso*

$\rho_{iso}$ = density for nuclide *iso*, in (g/cc)

$\sigma_{x,iso}(g,r)$ = microscopic cross section for reaction type x; of nuclide *iso*; in energy group *g*; at position *r*.

$\phi(g,r)$ = neutron flux in energy group g; at position r

$\psi(g,s)$ = neutron surface flux in energy group *g*; at surface position *s*

$\chi_{iso}(i,h)$ = delayed neutron fission spectrum of nuclide *iso*; for neutrons born in energy group *i*; to be deposited in delayed group *h*

$\Psi(i)$ = neutron flux in group *i* from fundamental mode calculation

$\Psi^{\dagger}(i)$ = adjoint flux in group *i* from fundamental mode calculation

**ACPU40: macroscopic capture cross-section for Pu-240**

$$ACPU40(g) = \frac{\int_{ass} N_{Pu-240}(r)\sigma_{c,Pu-240}(g,r)\phi(g,r)dr}{\int_{ass} \phi(g,r)dr}$$

**ADBI: lattice-averaged atomic number densities of each nuclide**

$$ADBI(m_{iso}) = \frac{1}{V_{ass}} \int_{ass} N_{iso}(r)dr$$

**ADBI41: lattice-averaged atomic number density of Pu-241**

$$ADBI41 = ADBI(m_{Pu-241} = 26)$$

**ADI : fuel-averaged atomic number density of heavy isotope iso**

$$ADI(m_{iso}) = \frac{1}{V_{fuel}} \int_{fuel} N_{iso}(r)dr$$

**ADP39 : fuel-averaged atomic number density of Pu-239**

$$ADP39 = ADI(m_{Pu-239} = 24)$$

**ADP40 : fuel-averaged atomic number density of Pu-240**

$$ADP40 = ADI(m_{Pu-240} = 25)$$

**ADP41 : fuel-averaged atomic number density of Pu-241**

$$ADP41 = ADI(m_{Pu-241} = 26)$$

**ADU : fuel-averaged atomic number density of all heavy isotopes**

$$ADU = \sum_{iso=heavy\ isotopes} ADI(m_{iso})$$

**ALAMDA : decay constant of delayed neutrons in delayed group h**

$$ALAMDA(h) = \frac{\sum_{iso=fissiles} \lambda_{iso}(h) \cdot \beta_{iso}(h) \cdot \sum_{g} N_{iso} \nu\sigma_{f,iso}(g)\phi(g)}{\bar{\beta}(h) \cdot \sum_{g} \nu\bar{\Sigma}_{f}(g)\phi(g)}$$

where $\beta_{iso}(h)$ is the delayed neutron fraction for nuclide *iso*, in delayed group *h*; and $\lambda_{iso}(h)$ is its decay constant. The averaged delayed neutron fraction, $\bar{\beta}(h)$, is calculated as,

$$\bar{\beta}(h) = \frac{\sum_{iso=fissiles} \beta_{iso}(h) \cdot \sum_{g} N_{sio} \nu\sigma_{f,iso}(g)\phi(g)}{\sum_{g} \nu\bar{\Sigma}_{f}(g)\phi(g)}$$

**AVLATF : few-group lattice-averaged flux**

$$AVLATF(g) = \frac{1}{V_{ass}} \int_{V_{ass}} \phi(g,r)dr$$

**BDC : few-group boundary diffusion coefficient for each assembly surface**

$$BDC(g) = \frac{\int_{S_{ass}} D(g,r)\psi(g,r)dS}{\int_{S_{ass}} \psi(g,r)dS}$$

where $\psi(g,r)$ is the surface flux at position $r$ and the integral is performed over one assembly surface only. There are 4 BDC values in the binary file: (1) north; (2) east; (3) south; (4) west.

**BETA : effective delayed neutron fraction for delayed group h**

The effective delayed neutron fraction accounts for the fact that delayed neutrons are born at energies lower than those of prompt neutrons and, hence, do not contribute to fast fission and have smaller leakage rates into (or out of) the system than prompt neutrons. The effective delayed neutron fraction is calculated as,

$$BETA(h) = \frac{\sum_{iso}\left[\sum_i \beta_{iso}(h)\bar{\chi}_{d,iso}(i,h)\Psi(i)\cdot\sum_i \nu\bar{\sigma}_{f,iso}(i)\bar{N}_{iso}\Psi(i)\right]}{\sum_{iso}\left\{\left(1-\sum_h \beta_{iso}(h)\right)\left(\sum_i \bar{\chi}_{p,iso}(i)\Psi^{\dagger}(i)\right)+\sum_h \beta_{iso}(h)\left(\sum_i \bar{\chi}_{d,iso}(i,h)\Psi^{\dagger}(i)\right)\right\}\cdot\sum_i \nu\bar{\Sigma}_f(i)\Psi(i)}$$

$$\cong \frac{\sum_{iso}\left[\sum_i \beta_{iso}(h)\bar{\chi}_{d,iso}(i,h)\Psi^{\dagger}(i)\cdot\sum_i \nu\bar{\sigma}_{f,iso}(i)\bar{N}_{iso}\Psi(i)\right]}{\sum_i \bar{\chi}(i)\Psi^{\dagger}(i)\cdot\sum_i \nu\bar{\Sigma}_f(i)\Psi(i)}$$

$$\cong \frac{\sum_{iso}\left[\sum_i \beta_{iso}(h)\bar{\chi}_{d,iso}(i,h)\Psi^{\dagger}(i)\cdot\sum_i \nu\bar{\sigma}_{f,iso}(i)\bar{N}_{iso}\Psi(i)\right]}{k^{\dagger}\sum_i \nu\bar{\Sigma}_f(i)\Psi(i)}$$

where the summation over *iso* includes the isotopes: $Th^{232}$, $U^{233}$, $U^{234}$, $U^{235}$, $U^{236}$, $U^{238}$, $Pu^{239}$, $Pu^{240}$, $Pu^{241}$, and $Pu^{242}$; $\bar{\chi}_{d,iso}(i,h)$ is the delayed neutron fission spectrum from energy group $i$ to delayed group $h$, for isotope *iso*; $\bar{\chi}_{p,iso}(i)$ is the prompt neutron fission spectrum for isotope *iso*; and $\bar{\chi}(i)$ is the total fission spectrum for the homogeneous system. The adjoint flux, $\Psi^{\dagger}(i)$, is obtained by solving the adjoint form of the fundamental mode equation,

$$\left[\bar{\Sigma}_{tr}(i)+\bar{D}(i)B^2\right]\cdot\Psi^{\dagger}(i) = \sum_{i'}\left[\bar{\Sigma}_s(i\rightarrow i')+\frac{\nu\bar{\Sigma}_f(i)}{k^{\dagger}}\cdot\bar{\chi}(i')\right]\Psi^{\dagger}(i')$$

where $B^2$ is the value of the material buckling from the solution to the forward form of the fundamental mode calculation; and the adjoint eigenvalue is given by,

$$k^{\dagger} = \sum_{i'} \bar{\chi}(i')\Psi^{\dagger}(i')$$

[[

]]

**BETAT : effective delayed neutron fraction (summed over 6 groups)**

$$BETAT = \sum_{h=1}^{6} BETA(h)$$

**C41 : lattice-averaged atomic number density of Pu-241**

$$C41 = ADBI(m_{Pu-241} = 26)$$

**CDFNN : few-group flux discontinuity factor for narrow-narrow corner**

$$CDFNN(g) = \frac{\psi(g, s = NN)}{\frac{1}{V_{ass}} \int_{V_{ass}} \phi(g,r)dr}$$

where $\psi(g, s = NN)$ is the few-group surface scalar flux in the SE (Narrow-Narrow) corner of the problem.

**CDFNW : few-group flux discontinuity factor for narrow-wide corner**

$$CDFNW(g) = \frac{\psi(g, s = NW)}{\frac{1}{V_{ass}} \int_{V_{ass}} \phi(g,r)dr}$$

where $\psi(g, s = NW)$ is the few-group surface scalar flux in the SW (Narrow-Wide) corner of the problem.

**CDFWW : few-group flux discontinuity factor for wide-wide corner**

$$CDFWW(g) = \frac{\psi(g, s = WW)}{\frac{1}{V_{ass}} \int_{V_{ass}} \phi(g,r)dr}$$

where $\psi(g, s = WW)$ is the few-group surface scalar flux in the NW (Wide-Wide) corner of the problem.

**D : few-group lattice-averaged diffusion coefficient**

$$D(g) = \sum_{i \in g} \left\{ \frac{\int_{V_{ass}} \phi(g,r)dr}{3 \int_{V_{ass}} \Sigma_{tr}(i,r)\phi(i,r)dr} \right\}$$

where the lattice-averaged diffusion coefficient is calculated in the fine-group energy structure and collapsed directly to the few-group energy structure.

**D41 : absorption reaction rate of Pu-241**

$$D41 = \sum_{g} \int_{V_{ass}} N_{Pu-241}(r)\sigma_{a,Pu-241}(g)\phi_g(r)dr$$

**DK41 : atomic number density reactivity coefficient of Pu-241**

$$DK41 = dK / dN_{Pu-241} - dK / dN_{Am-241} \doteq KINF \times \left( \frac{REALL(m_{Pu-241} = 26)}{ADBI(m_{Pu-241} = 26)} - \frac{REALL(m_{Am-241} = 27)}{ADBI(m_{Am-241} = 27)} \right)$$

**DNFA : lattice-averaged initial heavy metal density (g/cc)**

$$DNFA = \sum_{iso} A_{iso} \times ADBI_{iso} / N_{Avogadro}$$

**EPF : effective release energy per fission**

$$EPF = \frac{\int_{V_{fuel}} \left\{ F_{kinetic}(r) + F_{\gamma}(r) + F_{\beta}(r) - F_{c}(r) \right\} dr}{\sum_{g} \int_{V_{fuel}} \Sigma_{f}(g,r)\phi(g,r)dr}$$

where the energy terms are defined in equations (71) through (74).

**EX : exposure point in depletion calculation**

EX is the exposure array that corresponds to all other arrays in the Cedar file. It is a two dimensional array as a function of time step and void fraction.

**FDFN : few-group flux discontinuity factor along narrow gap**

$$FDFN(g) = \frac{\frac{1}{S_{narrow}} \int_{S_{narrow}} \psi(g,s)ds}{\frac{1}{V_{ass}} \int_{V_{ass}} \phi(g,r)dr}$$

**FDFW : few-group flux discontinuity factor along wide gap**

$$FDFW(g) = \frac{\frac{1}{S_{wide}} \int_{S_{wide}} \psi(g,s)ds}{\frac{1}{V_{ass}} \int_{V_{ass}} \phi(g,r)dr}$$

**FDR : fission detector response**

$$FDR = \sum_{i} \sigma_{f,m_{U-235}}(i)\phi(i, r = SE)$$

where $\phi(i, r = SE)$ is the fine-group scalar flux in the SE corner of the problem; and $\sigma_{f,U-235}(i)$ is the fine-group microscopic fission cross section for $U^{235}$.

**FFI : lattice-averaged fission fraction of TGBLA [17] isotope m (with GEBLA index)**

$$FFI_m = \frac{\sum_g \int_{V_{ass}} N_m(r)\sigma_{f,m}(g,r)\phi(g,r)dr}{\sum_g \int_{V_{ass}} \Sigma_f(g,r)\phi(g,r)dr}$$

**FFILNC : lattice-averaged fission fraction of LANCR isotope m (with LANCR index)**

Same definition as FFI.

**FFXR : fast flux fraction above 1 MeV**

$$FFXR = \frac{FLUX1}{FLUXS} \cdot FNF$$

**FLODAT : flow related data (e.g., areas, densities, wetted perimeters, etc.)**

FLODAT(1) = in-channel flow area (not including water rods) ($cm^2$).
FLODAT(2) = out-channel flow area (not including control blade) ($cm^2$).
FLODAT(3) = water rod flow area ($cm^2$).
FLODAT(4) = control blade flow area ($cm^2$).
FLODAT(5) = total flow area ($cm^2$).
FLODAT(6) = density of in-channel water ($g/cm^3$).
FLODAT(7) = density of out-channel water ($g/cm^3$).
FLODAT(8) = density of water in water rods ($g/cm^3$).
FLODAT(9) = density of water in control blade ($g/cm^3$).
FLODAT(10) = lattice-averaged water density ($g/cm^3$).
FLODAT(11) = heated perimeter of all fuel rods (cm).
FLODAT(12) = wetted perimeter of in-channel coolant (cm).
FLODAT(13) = hydraulic diameter of in-channel coolant (cm).

**FLUX1 : lattice-averaged fast flux (above 1 MeV)**

$$FLUX1 = \sum_{i=1}^{11} \Psi(i)$$

where the summation over energy group runs from [[
]]

**FLUX1C : fast flux (above 1 MeV) in the cladding of rod (x,y)**

$$FLUX1C(x,y) = \sum_{i=1}^{11} \phi(i,r)$$

where (x,y) represents a pin cell location; and $\phi(i,r)$ is the neutron flux in the clad region of the cell. The summation over energy group runs from [[
]]

**FLUXS : lattice-averaged absolute neutron flux**

$$FLUXS = \sum_{g} AVLATF(g)$$

**FLXLIB : fine-group critical spectrum from fundamental mode calculation**

$$FLXLIB(i) = \Psi(i)$$

where $\Psi(i)$ is the flux from the solution to Eq. (39).

**FNF : flux normalization factor**

$$FNF = \frac{\sum_{i} \int_{V_{ass}} \Sigma_f(i,r)\phi(i,r)dr}{\int_{V_{ass}} dr}$$

**Factor used to ratio the detector responses.**

**FRR : relative fission rate in rod (x,y)**

$$FRR(x,y) = \frac{\sum_{g} \int_{V_{x,y}} \Sigma_f(g,r)\phi(g,r)dr}{\left\{\frac{\sum_{g} \int_{V_{fuel}} \Sigma_f(g,r)\phi(g,r)dr}{\int_{V_{fuel}} dr}\right\}}$$

**GMNAME : name of gamma cross section library used for this state point**

Only the first 40 characters of the name are saved.

**GRR : relative gamma heating rate for rod (x,y)**

$$GRR(x,y) = \frac{\sum_j \int_{V_{x,y}} \Sigma_e(j,r)\phi(j,r)dr}{\left\{\frac{\sum_j \int_{V_{fuel}} \Sigma_e(j,r)\phi(j,r)dr}{\int_{V_{fuel}} dr}\right\}}$$

where $\Sigma_e(j,r)$ is the 8-group macroscopic energy deposition cross section for material region r.

[[

]]

[[

**where is the fine-group scalar flux in the SE corner of the problem; and is the fine-group microscopic fission cross section for U235. For the normalization factor, , P is the lattice power level, in MeV. [3]]]**

**KINF : infinite multiplication factor**

This is the multiplication factor obtained from the fine-group fundamental mode calculation following the two-dimensional MoC transport calculation.

**KINF3G : few-group infinite multiplication factor**

This is the multiplication factor obtained from the few-group cross sections. The few-group cross sections are created using the fine-group critical flux spectrum from the fundamental mode calculation.

$$KINF3G = \frac{\nu\bar{\Sigma}_f(1) + \nu\bar{\Sigma}_f(2)\cdot SI(2) + \nu\bar{\Sigma}_f(3)\cdot SI(3)}{\bar{\Sigma}_a(1) + \bar{\Sigma}_r(1)}$$

where the spectral indices are defined as,

$$SI(2) = \frac{\bar{\Sigma}_r(1)}{\bar{\Sigma}_a(2) + \bar{\Sigma}_r(2)}$$

and

$$SI(3) = \frac{\bar{\Sigma}_r(2)}{\bar{\Sigma}_a(3)}\cdot SI(2)$$

**LBNAME : name of neutron cross section library used for this state point**

**Only the first 40 characters of the name are used.**

**LNCR_INFO : LANCR02 information**

**DTIME = Time of execution (beginning of run).**

**UNAME = User name.**

**LNCRVR = LANCR02 version.**

**LBPATH = Library path name (cLibPath).**

**LBNAME = Name of neutron cross section Cedar file (cLibName).**

**LBLIST = Name of Cedar file defining nuclides contained in neutron cross section library (cLibList).**

**LBVERS = Cross section version (e.g., ENDF/B-VI, ENDF/B-VII, etc.).**

**GMNAME = Name of Cedar file containing gamma cross sections (cGammaLib).**

**LNCRCM = 5 lines of comments available to the programmer.**

**MOCINP : card input from MoC module**

A copy of the ASCII card input for the MoC solution.

**POLAT : power density**

Input power density.

**RCRA : neutron flux ratio of narrow-narrow corner rod to lattice average**

$$RCRA(g) = \frac{\phi(g, r = SE)}{AVLATF(g)}$$

where $\phi(g, r = SE)$ is the few-group scalar flux in the SE corner of the problem.

**REALL : reactivity worth of each nuclide**

Reactivity change when the atomic number density of each nuclide increases 100%.

$$REALL(m_{iso}) = \frac{\sum_g \int_{V_{ass}} N_{iso} \nu\sigma_{f,iso}(g,r)\phi(g,r)dr}{\sum_g \int_{V_{ass}} \nu\Sigma_f(g,r)\phi(g,r)dr} - \frac{\sum_g \int_{V_{ass}} N_{iso}\sigma_{a,iso}(g,r)\phi(g,r)dr}{\sum_g \int_{V_{ass}} \Sigma_a(g,r)\phi(g,r)dr}$$

**REB10 : reactivity worth of B-10**

$$REB10 = REALL(m_{B-10} = 41)$$

**REGD : reactivity worth of Gd-155 and Gd-157**

$$REGD = REALL(m_{Gd-155} = 149) + REALL(m_{Gd-157} = 151)$$

**RESM : reactivity worth of Sm-149**

$$RESM = REALL(m_{Sm-149} = 133)$$

**REXE : reactivity worth of Xe-135**

$$REXE = REALL(m_{Xe-135} = 98)$$

**REX : rod-wise relative exposure**

$$REX(x,y) = \frac{\text{expo}(x,y)}{\left\{ \dfrac{\int_{V_{fuel}} \text{expo}(x,y)dr}{\int_{V_{fuel}} dr} \right\}}$$

where expo$(x,y)$ is the integrated energy produced by the pin (in GWd) divided by the initial weight of actinides in the pin (in short tons).

**RHOB : reference water density (g/cc)**

$$RHOB = 0.73749$$

**RPR : rod-wise relative power**

$$RPR(x,y) = \frac{pow(x,y)}{\left\{ \dfrac{\int_{V_{fuel}} pow(x,y)dr}{\int_{V_{fuel}} dr} \right\}}$$

**RTIPA : ratio of TIP flux to lattice-averaged flux for few-group energy g**

$$RTIPA(g) = \frac{\phi(g, r = SE)}{AVLATF(g)}$$

**SAAM41 : lattice-averaged microscopic absorption cross-section of Am-241**

$$SAAM41(g) = \frac{\int_{V_{ass}} N_{Am-241}(r)\sigma_{a,Am-241}(g,r)\phi(g,r)dr}{\frac{1}{V_{ass}}\int_{V_{ass}} N_{Am-241}(r)dr \int_{V_{ass}} \phi(g,r)dr}$$

**SAPU41 : lattice-averaged microscopic absorption cross-section of Pu-241**

$$SAPU41(g) = \frac{\int_{V_{ass}} N_{Pu-241}(r)\sigma_{a,Pu-241}(g,r)\phi(g,r)dr}{\frac{1}{V_{ass}}\int_{V_{ass}} N_{Pu-241}(r)dr \int_{V_{ass}} \phi(g,r)dr}$$

**SASM : lattice-averaged microscopic thermal absorption cross-section of Sm-149**

$$SASM = \frac{\int_{V_{ass}} N_{Sm-149}(r)\sigma_{a,Sm-149}(3,r)\phi(3,r)dr}{\frac{1}{V_{ass}}\int_{V_{ass}} N_{Sm-149}(r)dr \int_{V_{ass}} \phi(3,r)dr}$$

**SCPU40 : lattice-averaged microscopic capture cross-section of Pu-240**

$$SCPU40(g) = \frac{\int_{V_{ass}} N_{Pu-240}(r)\sigma_{c,Pu-240}(g,r)\phi(g,r)dr}{\frac{1}{V_{ass}}\int_{V_{ass}} N_{Pu-240}(r)dr \int_{V_{ass}} \phi(g,r)dr}$$

**SAXE : lattice-averaged microscopic thermal absorption cross-section of Xe-135**

$$SAXE = \frac{\int_{V_{ass}} N_{Xe-135}(r)\sigma_{a,Xe-135}(3,r)\phi(3,r)dr}{\frac{1}{V_{ass}}\int_{V_{ass}} N_{Xe-135}(r)dr \int_{V_{ass}} \phi(3,r)dr}$$

**SFPU41 : lattice-averaged microscopic fission cross-section of Pu-241**

$$SFPU41(g) = \frac{\int_{V_{ass}} N_{Pu-241}(r)\sigma_{f,Pu-241}(g,r)\phi(g,r)dr}{\frac{1}{V_{ass}}\int_{V_{ass}} N_{Pu-241}(r)dr \int_{V_{ass}} \phi(g,r)dr}$$

**SPPU41 : lattice-averaged microscopic production cross-section of Pu-241**

$$SPPU41(g) = \frac{\int_{V_{ass}} N_{Pu-241}(r)\nu\sigma_{f,Pu-241}(g,r)\phi(g,r)dr}{\frac{1}{V_{ass}}\int_{V_{ass}} N_{Pu-241}(r)dr \int_{V_{ass}} \phi(g,r)dr}$$

**STATUS : final status of job**

**CLEAN = normal termination; blank = abnormal termination**

**TASD : Time after shutdown**

LANCR input data TASD.

**TEF : fuel temperature**

LANCR input data.

**TEMC : cladding temperature**

LANCR input data.

**TEMF : fuel temperature**

LANCR input data.

**TEM : in-channel coolant temperature**

**LANCR02 input data.**

**TEMOUT : out-channel coolant temperature**

**LANCR02 input data TEMPO.**

**U : instantaneous relative water density**

$$U = \frac{\int_{V_{ass}} \rho_{H_2O}(r)dr}{RHOB\ V_{H_2O}}$$

where $V_{H_2O}$ is the volume of all in-channel and out-channel water.

**UH : exposure-averaged relative water density**

$$UH = \frac{\int_0^E U(t)dt}{\int_0^E dt}$$

**UIN : instantaneous in-channel relative water density**

$$UIN = \frac{FLODAT(6)}{RHOB}$$

**UOUT : instantaneous out-channel relative water density**

$$UOUT = \frac{FLODAT(7)}{RHOB}$$

**UWR : instantaneous water rod relative water density**

$$UWR = \frac{FLODAT(8)}{RHOB}$$

**V : average few-group neutron velocity**

$$V(g) = \frac{\sum_{i \in g} \Psi^{\dagger}(i)}{\sum_{i \in g} \frac{\Psi^{\dagger}(i)}{v(i)}}$$

where $v(i)$ is the neutron velocity in the fine-group energy structure; and $\Psi^{\dagger}(i)$ is the adjoint flux from the fundamental mode solution (see the description for BETA(h) in this section).

**V,OPT2 : average few-group neutron velocity (calculated using critical forward flux)**

$$V(g) = \frac{\sum_{i \in g} \Psi(i)}{\sum_{i \in g} \frac{\Psi(i)}{v(i)}}$$

where $\Psi(i)$ is the critical forward flux from the fundamental mode solution.

**V,OPT3 : average few-group neutron velocity (calculated using infinite adjoint flux)**

$$V(g) = \frac{\sum_{i \in g} \Psi^{\dagger}(i)}{\sum_{i \in g} \frac{\Psi^{\dagger}(i)}{v(i)}}$$

where $\Psi^{\dagger}(i)$ is the infinite adjoint flux from the fundamental mode solution (no neutron leakage included).

**VF : void fraction**

LANCR02 input data.

VFIN : Void fraction

LANCR02 input data.

**VFOUT : Void fraction**

LANCR02 input data.

**VFWR : Void fraction**

LANCR02 input data.

**VFXY : Pin-wise void fraction**

This is the pin-wise void distribution used during the MoC solution. For most applications, the void is uniformly distributed across the in-channel area. However, the user has the option of entering a non-uniform void distribution or instructing the code to calculate a non-uniform void distribution based on distributed void model.

**WFI : lattice-averaged weight fraction of GTHERM isotope to initial heavy elements (with GEBLA index)**

$$WFI(m_{iso}) = \frac{\int_{V_{ass}} A_{iso} N_{iso}(r) dr}{\sum_{iso=1}^{30} \int_{V_{ass}} A_{iso} N_{iso}^{BOL}(r) dr}$$

where the value of m for heavy metals encompasses $Th^{228}$ through $Am^{242}$.

**WFILNC : lattice-averaged weight fraction of GTHERM isotope to initial heavy elements (with LANCR index)**

$$WFI(m_{iso}) = \frac{\int_{V_{ass}} A_{iso} N_{iso}(r) dr}{\sum_{iso=1}^{40} \int_{V_{ass}} A_{iso} N_{iso}^{BOL}(r) dr}$$

where the value of m for heavy metals encompasses $Th^{228}$ through $Cm^{246}$.

**XA : few-group lattice-averaged absorption cross section**

$$XA(g) = \frac{\sum_{i \in g} \int_{V_{ass}} \Sigma_a(i,r) \phi(i,r) dr}{\sum_{i \in g} \int_{V_{ass}} \phi(i,r) dr}$$

**XAMXE : lattice-averaged thermal absorption cross section minus the Xe contribution**

$$XAMXE = XA(g) - SAXE \times ADBI_{m=98}$$

**XF : few-group lattice-averaged fission cross section**

$$XF(g) = \frac{\sum_{i \in g} \int_{V_{ass}} \Sigma_f(i,r) \phi(i,r) dr}{\sum_{i \in g} \int_{V_{ass}} \phi(i,r) dr}$$

**XFCRT : microscopic fission cross section at instrument location**

$$XFCRT(g) = \frac{\sum_{i \in g} \sigma_{f,U-235}(i)\phi(i,r')}{\sum_{i \in g} \phi(i,r')}$$

where $r'$ is the location of the instrument tube in the SE water gap corner of the problem. The microscopic fission cross section is the unshielded (i.e., infinitely dilute) value.

**XNF : few-group lattice-averaged production cross section**

$$XNF(g) = \frac{\sum_{i \in g} \int_{V_{ass}} \nu\Sigma_f(i,r)\phi(i,r)dr}{\sum_{i \in g} \int_{V_{ass}} \phi(i,r)dr}$$

**XSC : few-group lattice-averaged scattering kernel**

$$XSC(g',g) = \frac{\sum_{i \in g} \sum_{i' \in g'} \int_{V_{ass}} \Sigma_s(i',i,r)\phi(i',r)dr}{\sum_{i \in g} \sum_{i' \in g'} \int_{V_{ass}} \phi(i',r)dr}$$

where $XSC(g',g)$ is the scattering cross section from group $g'$ to group g.

**XSL : few-group lattice-averaged removal cross section**

$$XSL(1) = \frac{\nu\bar{\Sigma}_f(1) + \nu\bar{\Sigma}_f(2)\cdot\frac{\bar{\phi}(2)}{\bar{\phi}(1)} + \nu\bar{\Sigma}_f(3)\cdot\frac{\bar{\phi}(3)}{\bar{\phi}(1)}}{k^{\infty}} - \bar{\Sigma}_a(1)$$

$$XSL(2) = XSL(1)\cdot\frac{\bar{\phi}(1)}{\bar{\phi}(2)} - \bar{\Sigma}_a(2)$$

$$XSL(3) = 0$$

where the few-group eigenvalue is calculated as,

$$k^{\infty} = \frac{\nu\bar{\Sigma}_f(1)\cdot\bar{\phi}(1) + \nu\bar{\Sigma}_f(2)\cdot\bar{\phi}(2) + \nu\bar{\Sigma}_f(3)\cdot\bar{\phi}(3)}{\bar{\Sigma}_a(1)\cdot\bar{\phi}(1) + \bar{\Sigma}_a(2)\cdot\bar{\phi}(2) + \bar{\Sigma}_a(3)\cdot\bar{\phi}(3)}$$

[[

]]

**XTRLIB : fine-group lattice-averaged transport cross section**

$$XTRLIB(i) = \frac{\int_{V_{ass}} \Sigma_{tr}(i,r)\phi(i,r)dr}{\int_{V_{ass}} \phi(i,r)dr}$$

**XYLOC : location of fuel pin relative to wide-wide corner**

XYLOC(1,x,y) : x-coordinate of pin (x,y)

XYLOC(2,x,y) : y-coordinate of pin (x,y)

**YBA140 : average fission yield of Ba-140**

$$YBA140 = \frac{\sum_{iso=1}^{40} \int_{V_{fuel}} Y_{m',Ba-140} N_{iso}(r)\sigma_{f,iso}(g,r)\phi(g,r)dr}{\sum_{iso=1}^{40} \int_{V_{fuel}} N_{iso}(r)\sigma_{f,iso}(g,r)\phi(g,r)dr}$$

where $Y_{iso,Ba-140}$ is the yield from actinide *iso* to $Ba^{140}$; and the summation is performed over all actinides $Th^{228}$ through $Cm^{246}$.

**YCE140 : average fission yield of Ce-144**

$$YCE140 = \frac{\sum_{iso=1}^{40} \int_{V_{fuel}} Y_{iso,Ce-144} N_{iso}(r)\sigma_{f,m}iso(g,r)\phi(g,r)dr}{\sum_{iso=1}^{40} \int_{V_{fuel}} N_{iso}(r)\sigma_{f,iso}(g,r)\phi(g,r)dr}$$

where $Y_{iso,Ce-144}$ is the yield from actinide *iso* to $Ce^{144}$; and the summation is performed over all actinides $Th^{228}$ through $Cm^{246}$.

**YI : average fission yield of I-135**

$$YI = \frac{\sum_{iso=1}^{40} \int_{V_{fuel}} Y_{iso,I-135} N_{iso}(r) \sigma_{f,iso}(g,r) \phi(g,r) dr}{\sum_{iso=1}^{40} \int_{V_{fuel}} N_{iso}(r) \sigma_{f,iso}(g,r) \phi(g,r) dr}$$

where $Y_{iso,I-135}$ is the yield from actinide *iso* to $I^{135}$; and the summation is performed over all actinides $Th^{228}$ through $Cm^{246}$.

**YPM : average fission yield of Pm-149**

$$YPM = \frac{\sum_{iso=1}^{40} \int_{V_{fuel}} Y_{iso,Pm-149} N_{m'}(r) \sigma_{f,iso}(g,r) \phi(g,r) dr}{\sum_{iso=1}^{40} \int_{V_{fuel}} N_{iso}(r) \sigma_{f,iso}(g,r) \phi(g,r) dr}$$

where $Y_{iso,Pm-149}$ is the yield from actinide *iso* to $Pm^{149}$; and the summation is performed over all actinides $Th^{228}$ through $Cm^{246}$.

**YRU105 : average fission yield of Ru-105**

$$YRU105 = \frac{\sum_{iso=1}^{40} \int_{V_{fuel}} Y_{iso,Ru-105} N_{iso}(r) \sigma_{f,iso}(g,r) \phi(g,r) dr}{\sum_{iso=1}^{40} \int_{V_{fuel}} N_{iso}(r) \sigma_{f,iso}(g,r) \phi(g,r) dr}$$

where $Y_{iso,Ru-105}$ is the yield from actinide *iso* to $Ru^{105}$; and the summation is performed over all actinides $Th^{228}$ through $Cm^{246}$.

**YXE : average fission yield of Xe-135**

$$YXE = \frac{\sum_{iso=1}^{40} \int_{V_{fuel}} Y_{iso,Xe-135} N_{iso}(r) \sigma_{f,iso}(g,r) \phi(g,r) dr}{\sum_{iso=1}^{40} \int_{V_{fuel}} N_{iso}(r) \sigma_{f,iso}(g,r) \phi(g,r) dr}$$

where $Y_{iso,Xe-135}$ is the yield from actinide *iso* to $Xe^{135}$; and the summation is performed over all actinides $Th^{228}$ through $Cm^{246}$.

# 10. Applicable Documentation

[1] D. KNOTT, et al., "Description of the LANCER02 Lattice Physics Code for Single-Assembly and Multibundle Analysis," *Nuclear Science and Engineering*, Vol. 155, p. 331-354, (2007).

[2] R.E. MACFARLANE and D.W. MUIR, "The NJOY Nuclear Data Processing System, Version 91," LA-12740-M, Los Alamos National Laboratory, Los Alamos, N.M. (1994).

[3] J. R. Lamarsh, *Nuclear Reactor Theory*, Addison-Wesley Publishing Co., 1966.

[4] E.P. WIGNER, et al., *J. Appl. Phys.*, Vol. 2, pp. 257, 260, 271, (1955).

[5] C. C. STOKER and Z. J. WEISS, "Spatially Dependent Resonance Cross Sections in a Fuel Rod," *Ann. Nucl. Energy*, Vol. 23, No. 9, pp. 765-778 (1996).

[6] N. Sugimura and A. Yamamoto, "Evaluation of Dancoff Factors in Complicated Geometry Using the Method of Characteristics," Original paper submitted for publication to the *Journal of Nuclear Science and Engineering*, (2006).

[7] A. HÉBERT, "A Review of Legacy and Advanced Self-Shielding Models for Lattice Calculations," *Intl. Topl. Mtg. on Math. & Comp.*, Avignon, France, (2005).

[8] M. L. WILLIAMS, "Correction of Multigroup Cross Sections for Resolved Resonance Interference in Mixed Absorbers," *Nuclear Science and Engineering*, Vol. 83, p. 37-40 (1983).

[9] E. WEHLAGE, et al., "Modeling Resonance Interference Effects in the Lattice Physics Code LANCER02," *Intl. Topl. Mtg. on Math. & Comp.*, Avignon, France, (2005).

[10] D. KNOTT, "KRAM, A Lattice Physics Code for Modeling the Detailed Depletion of Gadolinia Isotopes from BWR Fuel Designs," PhD Thesis, The Pennsylvania State University, University Park, PA, (1991).

[11] I. CARLVIK, "Integral Transport Theory in One-Dimensional Geometries," Part of Carlvik's PhD Thesis, Chalmers University, Göteborg, Sweden, AE-227, (1966).

[12] I. CARLVIK, "A Method for Calculating Collision Probabilities in General Cylindrical Geometry and Applications to Flux Distributions and Dancoff Factors," Part of Carlvik's PhD Thesis, Chalmers University, Göteborg, Sweden, (1966).

[13] E. E. LEWIS and W. F. MILLER, JR., "*Computational Methods of Neutron Transport*," John Wiley & Sons, Inc., (1984).

[14] J. R. ASKEW, "A Characteristics Formulation of the Neutron Transport Equation in Complicated Geometries," AEEW-M 1108, (1972).

[15] M. Tabuchi, A. Yamamoto, and T. Endo, "Yet Another Optimum Polar Angle Quadratre Set for the Method of Characteristics," *Trans. Am. Nucl. Soc.*, 93, (2005).

[16] D. KNOTT and M. EDENIUS, "Validation of the Casmo-4 Transport Solution," *Proc. of the Joint Intnl. Conf. on Math. Meth. and Supercomp. in Nucl. Apps.*, Karlsruhe, Germany (1993).

[17] S. Richards (NRC) to G. Watford (GE), MFN-035-99, Amendment 26 to GE Licensing Topical Report NEDE-24011-P-A, *"GESTAR II" – Implementing Improved GE Steady State Methods (TAC No. MA6481)*, November 10, 1999.

# ENCLOSURE 3

# FLN-2007-028

# Affidavit

# Global Nuclear Fuel – Americas

# AFFIDAVIT

**I, Andrew A. Lingenfelter,** state as follows:

(1) I am Vice President, Fuel Engineering, Global Nuclear Fuel – Americas, L.L.C. ("GNF-A"), and have been delegated the function of reviewing the information described in paragraph (2) which is sought to be withheld, and have been authorized to apply for its withholding.

(2) The information sought to be withheld is contained in the GE Topical Report NEDC-33376P, Revision 0, "LANCR02 LATTICE PHYSICS MODEL DESCRIPTION" Class III (GNF-A Proprietary Information), dated September 2007. The proprietary information in "Attachment, Enclosure, Subject of Letter, Report", date, is identified by [[a dotted underline inside double square brackets$^{\{3\}}$]]. Figures and other large objects are identified with double square brackets before and after the object. In each case, the superscript notation {3} refers to Paragraph (3) of this affidavit, which provides the basis for the proprietary determination.

(3) In making this application for withholding of proprietary information of which it is the owner or licensee, GNF-A relies upon the exemption from disclosure set forth in the Freedom of Information Act ("FOIA"), 5 USC Sec. 552(b)(4), and the Trade Secrets Act, 18 USC Sec. 1905, and NRC regulations 10 CFR 9.17(a)(4), and 2.390(a)(4) for "trade secrets" (Exemption 4). The material for which exemption from disclosure is here sought also qualify under the narrower definition of "trade secret", within the meanings assigned to those terms for purposes of FOIA Exemption 4 in, respectively, Critical Mass Energy Project v. Nuclear Regulatory Commission, 975F2d871 (DC Cir. 1992), and Public Citizen Health Research Group v. FDA, 704F2d1280 (DC Cir. 1983).

(4) Some examples of categories of information which fit into the definition of proprietary information are:

a. Information that discloses a process, method, or apparatus, including supporting data and analyses, where prevention of its use by GNF-A's competitors without license from GNF-A constitutes a competitive economic advantage over other companies;

b. Information which, if used by a competitor, would reduce his expenditure of resources or improve his competitive position in the design, manufacture, shipment, installation, assurance of quality, or licensing of a similar product;

c. Information which reveals aspects of past, present, or future GNF-A customer-funded development plans and programs, resulting in potential products to GNF-A;

d. Information which discloses patentable subject matter for which it may be desirable to obtain patent protection.

The information sought to be withheld is considered to be proprietary for the reasons set forth in paragraphs (4)a. and (4)b. above.

(5) To address 10 CFR 2.390 (b) (4), the information sought to be withheld is being submitted to NRC in confidence. The information is of a sort customarily held in confidence by GNF-A, and is in fact so held. The information sought to be withheld has, to the best of my knowledge and belief, consistently been held in confidence by GNF-A, no public disclosure has been made, and it is not available in public sources. All disclosures to third parties including any required transmittals to NRC, have been made, or must be made, pursuant to regulatory provisions or proprietary agreements which provide for maintenance of the information in confidence. Its initial designation as proprietary information, and the subsequent steps taken to prevent its unauthorized disclosure, are as set forth in paragraphs (6) and (7) following.

(6) Initial approval of proprietary treatment of a document is made by the manager of the originating component, the person most likely to be acquainted with the value and sensitivity of the information in relation to industry knowledge, or subject to the terms under which it was licensed to GNF-A. Access to such documents within GNF-A is limited on a "need to know" basis.

(7) The procedure for approval of external release of such a document typically requires review by the staff manager, project manager, principal scientist or other equivalent authority, by the manager of the cognizant marketing function (or his delegate), and by the Legal Operation, for technical content, competitive effect, and determination of the accuracy of the proprietary designation. Disclosures outside GNF-A are limited to regulatory bodies, customers, and potential customers, and their agents, suppliers, and licensees, and others with a legitimate need for the information, and then only in accordance with appropriate regulatory provisions or proprietary agreements.

(8) The information identified in paragraph (2) is classified as proprietary because it contains detailed results of analytical models, methods, and processes, including computer codes which would provide other parties, including competitors, with information related GNF-A (*fuel designs, analysis results and potential commercial offerings for the BWR plant design*) which were developed at considerable expense to GNF-A

The development of the evaluation process, along with the interpretation and application of the analytical results is derived from the extensive experience database that constitutes a major asset to GNF-A.

(9) Public disclosure of the information sought to be withheld is likely to cause substantial harm to GNF-A's competitive position and foreclose or reduce the availability of profit-making opportunities. The information is part of GNF-A's comprehensive BWR safety and technology base, and its commercial value extends beyond the original development cost. The value of the technology base goes beyond the extensive physical database and analytical methodology and includes development of the expertise to determine and apply the appropriate evaluation process. In addition, the technology base includes the value derived from providing analyses done with NRC-approved methods.

The research, development, engineering, analytical, and NRC review costs comprise a substantial investment of time and money by GNF-A.

The precise value of the expertise to devise an evaluation process and apply the correct analytical methodology is difficult to quantify, but it clearly is substantial.

GNF-A's competitive advantage will be lost if its competitors are able to use the results of the GNF-A experience to normalize or verify their own process or if they are able to claim an equivalent understanding by demonstrating that they can arrive at the same or similar conclusions.

The value of this information to GNF-A would be lost if the information were disclosed to the public. Making such information available to competitors without their having been required to undertake a similar expenditure of resources would unfairly provide competitors with a windfall, and deprive GNF-A of the opportunity to exercise its competitive advantage to seek an adequate return on its large investment in developing and obtaining these very valuable analytical tools.

I declare under penalty of perjury that the foregoing affidavit and the matters stated therein are true and correct to the best of my knowledge, information, and belief.

Executed on this 6th day of September 2007.

Andrew A. Lingenfelter
Manager, Engineering
Global Nuclear Fuel – Americas, L.L.C.